Microstructure scale modelling of the WC and Co phases plastic behaviour in the WC-Co composite with different cobalt contents and for different temperatures. Comparison of the Drucker-Prager and Mises models

K.E. Agode, C. Wolff, M. Nouari, A. Moufki

Microstructure scale modelling of the WC and Co phases plastic behaviour in the WC-Co composite with different cobalt contents and for different temperatures. Comparison of the Drucker Prager and Mises models

K. E. Agode[1], C. Wolff[1*], M. Nouari[1], A. Moufki[2]

[1]*Université de Lorraine, CNRS, LEM3, IMT, GIP InSIC, F-88100 Saint Dié des Vosges, France.*

[2]*Université de Lorraine, CNRS, Arts et Métiers ParisTech LEM3 F-57070 Metz, France.*

[*]*Corresponding author Cyprien Wolff,* cyprien.wolff@univ-lorraine.fr

Abstract

Despite several years of research and development works, the understanding of the tungsten carbide (WC-Co) behaviour under complex thermomechanical loading is not yet complete. Indeed, data is quite rare for the elevated temperatures encountered in the various applications and makes the description of this material a difficult task. In the present work, the elastoplastic behaviour of various grades of WC-Co composites are simulated numerically from room temperature up to 900°C thanks to the creation of realistic microstructures. This microstructure-level model allows to determine the representative volume element (RVE) considering the two phases tungsten carbide (WC) and cobalt (Co) to reproduce the real macroscopic behaviour of the composite under compression loading. The elastoplastic behaviour of the Co phase has been identified from the literature and the yield criterion of WC phase estimated at different temperatures by the introduction and determination of two temperature functions $\alpha_1(T)$ and $\alpha_2(T)$. These two functions represent the dependence of the yield stress and hardening, respectively. A comparison between the von Mises and Drucker Prager criteria applied to the WC phase has been also discussed. A good agreement is obtained between the numerical simulation results and experimental data.

Keywords: *WC-Co hard metal, Microstructure model, Plastic deformation, Temperature dependent behaviour, Finite element analysis.*

1. Introduction

Tungsten carbide (WC) is the main material used for more than 70% of cutting tools and tooling materials due to its high hardness, mechanical strength and abrasion resistance [1]. WC-Co cemented carbides are the most common basic composition for cutting tools. Almost 95 years after the first Schroter's WC-Co composite having low porosity and good toughness [2], this material has been extensively developed to respond to industrial needs, and has resulted in all the grades known today. The high mechanical and thermal performance of WC-Co are the result of a combination of ductile

Cobalt (Co) binder and hard-brittle carbide (WC) grains [3–5] which is sintered around 1400°C [2]. Thus, the mechanical properties depend on many parameters such as the increase in hardness as the WC grain size and the weight percentage of Co (wt.%) decrease. In general, the WC grain size of ranges from 0.5 to 2 μm with a cobalt weight percentage ranging from 5 to 16% [6]. However, for some specific applications, such as the machining of metals or hard superalloys for example, the percentage by weight of cobalt is most of the time lower than 10%, according to the literature.

Many researches and development works mainly experimental have been conducted on the whole the supply chain of the initial WC-Co tool, from their manufacturing process to their breakdown (the end of their lifetime) [7–9]. Several authors have been particularly interested in behaviour of these WC-Co tools under extreme thermal and mechanical loadings [10–12] encountered in machining. For instance, in the investigation led by Davies et *al.* [13], a temperature of 1000°C along the tool-chip contact was achieved due to an intense friction during the machining of the AISI 1045 steel with a cutting speed of 605 $m.min^{-1}$ and uncut chip thicknesses of 133 μm. In addition, a temperature gradient in the tool was observed especially from the tool tip to the end of the tool-chip contact and also to the center of the tool where the temperature decreases. Many studies have been carried out on the WC-Co behaviour under large range of temperatures between 25 °C and 1000°C. Ueda et *al.* [11] and Emani et *al.* [14] identified three main temperature ranges where the WC/Co carbide tool exhibits different mechanical behaviours. In the range of 25 °C to 527 °C, Mari [15] observed a brittle and elastic WC-Co behaviour explained by the multiple intersections of stacking faults in the cobalt phase blocking the crystal lattice and inhibiting any movement [16]. From 527 °C to 827 °C, an increase of toughness induced by the softening of cobalt with a limited plastic deformation were observed. For temperatures over 827 °C and below 1000°C, the sliding of the WC grain boundaries is one of the mechanisms involving the softening of WC-Co subjected to larger plastic deformations.

In parallel with the experimental studies, the numerical simulation approach was also used to analyse the contribution of each phase in the mechanical behaviour of WC-Co at the microstructure scale. This work can be classified into two groups. The first group concerns the simulation of damaged WC-Co [17, 18]. The second one models the elasto-plastic behaviour of WC-Co prior to damage and on which the present study focuses. Without being exhaustive, some significant studies of this second group are recalled in the following, before introducing the subject of this paper.

In 1972 Jaensson et *al.* [19] proposed the first finite element simulations to compute the Young's modulus and Poisson's ratio of the WC-Co composite from 2D representative volume elements (RVE). These RVE were created from realistic microstructures composed of 20-30 carbides grains. Each phase has an elastic behaviour. A good agreement between experimental data and simulation results for different percentages of cobalt (1-30wt.%) was found. Thereafter, this work was extended by Sundstrom [20] to simulate the elasto-plastic behaviour of the composite in compression. Elasto-

plastic and elastic models were used for cobalt and WC, respectively. The results revealed that the plastic deformations are possible in the cobalt binder despite the presence of WC hard matrix phase. In addition, local plastic strains can reach twice times the value of the effective plastic strain. Twenty years later, Poech et *al.* [21] evaluated the possible impact of the microstructural parameters such as the shape and arrangement of the binder phase on the elasto-plastic behaviour of the WC-Co. The results show that these parameters have a slight influence on the strain-stress curves. The authors analysed the effect of the mesh geometry, mesh density and model size on the results. They showed that the yield stress of the composite decreases to a constant value for the densest meshes. Later, and thanks to more computing power, Sadowski et *al.* [22] performed numerical simulations on several sizes of representative surface features (RSE) or 2D RVE much larger than those used in previous works. They contain many grains (>120 grains for a RSE size of 10x10 μm) and are created from real microstructures. The best fit to the experimental data was obtained with the largest RSE (40x40 μm) under conditions of generalized plane strain. In a continuation of previous work, Chen et *al.* [23] proposed a statistical method for defining the minimum size of the 2D representative volume element of the WC-Co alloy and found that the RVE for a plastic study must be larger than that for an elastic study. The mean value of each parameter considered as the effective elastic constants or the anisotropic parameter converge from a RVE size of 30x30 μm but their respective standard deviation decreases further. From the obtained results, a RVE size of 40x40 μm is recommended by the authors. However, in the previous studies, the compression of the WC-Co is limited to strains lower than 0.6%. According to Poech et *al.* [21], after the initial plasticity of the composite, it is necessary to consider both the plastic and damage processes in the carbide phase. Tkalich et *al.* [24] proposed to simulate only the plasticity of the carbide with Drucker-Prager's isotropic model. This model is able to reproduce the difference in strength of the WC material under compression and tension. In their work, the elasto-plastic behaviour of the composite was simulated using a 2D RVE based on realistic microstructures and under generalized strain plane conditions. The decrease in strain rate after initial plasticity, often observed in the literature, is well reproduced. The authors then extended their model in another study [25] to an idealized 3D RVE created from an algorithm based on Voronoi cells. Several complex mechanical loads were applied on this RVE to estimate the shape of the initial elasticity surface of different WC-Co composites which is similar to a Drucker-Prager surface with a cap. However, for all numerical studies presented in this introduction, the simulations were performed at room temperature. As mentioned above, the WC-Co cutting tool is subjected to high temperatures up to 1000°C, which can change the mechanical behaviour of the composite. Recently, Faksa et *al.* [26] simulated the elasto-plastic behaviour of the WC-6wt.%Co composite in compression for the temperature range of 20 to 900 °C using a 2D RVE. Due to a lack of data, the pure Co was substituted by a cobalt alloy. The first results of the study showed that only the elasto-plastic behaviour of Co is insufficient to represent the plasticity of the composite for strains above 0.6% in the case of elastic WC behaviour. Therefore, a plastic behaviour was assumed for the WC phase. The stress-strain curves

of the WC are inversely reconstructed from the composite behaviour. However, this study is limited to WC-6wt.%Co composite.

This state of the art reveals the need to clarify the different behaviours of the tungsten carbide phase used in the literature. Although data on the elasto-plastic behaviour of WC are scarce, it is possible to identify it by an inverse approach similar to that adopted by Faksa et *al.* [26] with a pure cobalt phase. Finally, a finite element analysis of the elasto-plastic behaviour of WC-Co hard metal at the microstructural scale needs to be developed for different temperatures and cobalt contents. These shortcomings, mentioned above, are the subject of the present study.

This paper is structured as follow:

In Section 2, the elasto-plastic models to simulate the behaviour of the cobalt and WC phases are presented. For the carbide phase, the von Mises and Drucker Prager criteria used in the work of Tkalich et *al.* [24, 25] are proposed but only at room temperature. Then, in Section 3, an algorithm to generate idealized WC-Co microstructures is described. The advantage of this strategy is to control the cobalt content and the number of WC grains. In Section 4, a study is carried out to establish the number of WC grains necessary to build an RVE for the elasto-plastic behaviour of the composite at room temperature. Then, in Section 5, a temperature-dependent hardening law for the WC phase is determined from the behaviour of the composite WC-6 wt.%Co and the pure cobalt. The model is tested for a WC-10.5wt.% Co composite in uniaxial compression and the results are compared with literature data. Finally, a comparison between the von Mises and Drucker-Prager criteria applied to the WC phase is carried out. Some conclusions from this study are then given.

2. Modelling of the Co and WC phases behaviour

The modelling of the WC-Co elastoplastic behaviour at the microstructure scale requires suitable behaviour models dedicated to the Co and WC phases.

2.1 Elastic behaviour

The ductile phase of the cobalt is polycrystalline with a crystallite size of 3 times larger than that of the WC grains [27]. Its elastic behaviour is assumed to be isotropic. The Young's modulus and thermal expansion as a function of the temperature are taken from data given by Betteridge in [28] and Fine and Ellis in [29], see Figure 1. The Poisson's ratio is taken equal to 0.31 from the work of Poech et *al.* [21] since Teppernegg et *al.* [30] have shown its insensitivity to the temperature evolution.

The WC phase consists of several grains. Each grain has a transversely isotropic elastic behaviour due to its hexagonal crystal structure. However, most studies in literature [31, 32] using microstructural simulations of the WC-Co composite assume that each grain has the isotropic elastic behaviour of the polycrystal WC. This hypothesis is also chosen in the present study. The Young's modulus and

thermal expansion as a function of temperature are given in Figure 2 and are taken from [21] and [33]. The Poisson's ratio taken insensitive to the temperature is equal to 0.194 [21].

2.2 Plastic Model

In this section, the elasto-plastic model for the cobalt is presented. As mentioned in Introduction, in the models, the plasticity of the composite is mainly due to the plasticity of the cobalt phase, whereas the WC phase is often considered as an elastic medium. However, some authors [24, 26] assumed an elasto-plastic behaviour of the WC phase justified in the literature by the presence of slip marks observed in WC grains [34–36] or by a disorientation of WC grains observed in a deformed WC-6wt.%Co sample indicating some extension of plastic deformation [26]. Two elasto-plastic models of the WC used by these authors are also introduced in the following and will be compared and discussed later in this paper.

2.2.1 von Mises criterion for Cobalt and WC phases

The von Mises criterion usually used for metallic materials is adopted here for the cobalt phase. In a first approach, von Mises criterion can be transposed to the carbide phase. Faksa et *al.* [26] also adopted a plastic behaviour for both phases in ABAQUS software [37] that is based on the von Mises criterion. In the elasto-plastic regime of a phase "*i*" ($i = \text{carbide phase } WC$, cobalt phase C_o), von Mises criterion is chosen to describe its yield surface which is defined by:

$$f_i(\boldsymbol{\sigma}, p) = J_2(\boldsymbol{\sigma}) - (R_i + Y_i(p)) \tag{1}$$

with $J_2(\boldsymbol{\sigma}) = \sqrt{\frac{3}{2}\boldsymbol{s}:\boldsymbol{s}}$ the von Mises stress computed operator from $\boldsymbol{s} = \boldsymbol{\sigma} - \frac{1}{3}\text{trace}(\boldsymbol{\sigma})$ the deviatoric part of the stress tensor $\boldsymbol{\sigma}$. Bold letters are used to denote vectors and tensors. R_i and $Y_i(p)$, respectively, the yield stress and the isotropic hardening with p is the accumulated plastic strain which is defined by:

$$p = \int_0^t \sqrt{\frac{2}{3}\dot{\boldsymbol{\varepsilon}}^{\boldsymbol{p}}:\dot{\boldsymbol{\varepsilon}}^{\boldsymbol{p}}}\, dt \tag{2}$$

with, $\dot{\boldsymbol{\varepsilon}}^{\boldsymbol{p}}$ the plastic strain rate tensor and ":" the double contraction operator.

$\dot{\boldsymbol{\varepsilon}}^{\boldsymbol{p}}$ is calculated from the following associate flow rule:

$$\dot{\boldsymbol{\varepsilon}}^{\boldsymbol{p}} = \dot{\lambda}\frac{\partial g_i}{\partial \boldsymbol{\sigma}} \tag{3}$$

with $\dot{\lambda}$, the plastic multiplier and g_i flow potential defined which is equal to f_i from Equation (1).

The term $R_i + Y_i(p)$ describes a plastic stress-strain curve that can be obtained from a tensile or compression test. For the Co phase, these curves were measured in compression by Park et *al.* [38] for different temperatures, see Figure 3, and then described by a series of points written in a table in the ABAQUS software. The intermediate data between two points are calculated by linear interpolation. In the case of WC ($i = WC$), the term $R_{WC} + Y_{WC}(p)$ is taken from Tkalich et *al.* [24] where the isotropic hardening $Y_{WC}(p)$ is defined as follows:

$$Y_{WC}(p) = Q_{WC}[1 - \exp(-b_{WC}p)] \quad (4)$$

where Q_{WC} and b_{WC} are the hardening constants. The values of parameters $Rwc = 4000\ MPa$, $Qwc = 3000\ MPa$ and $bwc = 10$ are given for a uniaxial compression loading of the WC.

2.2.2 Drucker Prager criterion for the carbide WC phase

Tkalich et al. [24] used the Drucker Prager model [39] for the WC phase initially developed for soil mechanics. Thanks to its dependence on pressure, this model can reproduce the difference in behaviour between tension and compression. This difference is highlighted by the experiments carried out by Doi *et al*. [40] where tensile tests not exceed 0.7% of deformation and a maximal tensile stress of 210 MPa while compression tests reach the maximum of 4% of deformation and a maximal compressive stress of 335 MPa for a WC-20wt.% Co with a WC grain size of 2.1 µm. In the present work, this criterion, already implemented in ABAQUS code, is also adopted for the carbide phase to compare it with the von Mises criterion presented above.

The Drucker Prager criterion is defined as follows:

$$f_{WC}(\boldsymbol{\sigma}, p) = \sigma_{eq} - (R_{WC} + Y_{WC}(p)) \quad (5)$$

where the equivalent stress is $\sigma_{eq} = \frac{J_2(\boldsymbol{\sigma}) + I_1(\boldsymbol{\sigma})\tan(\phi_{WC})/3}{1 - \tan(\phi_{WC})/3}$ with $I_1(\boldsymbol{\sigma})$ =trace($\boldsymbol{\sigma}$) is the stress tensor trace and ϕ_{WC}, the friction angle that is set to 45°, implying that the yield stress in uniaxial tension is half as large as in compression [24]. In Equation (5), the term $R_{WC} + Y_{WC}(p)$ is given by Equation (4). The accumulated plastic strain p which is defined by :

$$p = \int_0^t \frac{\boldsymbol{\sigma} : \dot{\boldsymbol{\varepsilon}}^{\boldsymbol{p}}}{\sigma_{eq}} dt \quad (6)$$

the plastic strain rate $\dot{\boldsymbol{\varepsilon}}^{\boldsymbol{p}}$ is calculated from the following non-associated flow rule :

$$\dot{\boldsymbol{\varepsilon}}^{\boldsymbol{p}} = \dot{\lambda} \frac{\partial g_{WC}}{\partial \boldsymbol{\sigma}} \quad (7)$$

with $\dot{\lambda}$, the plastic multiplier and g_{WC} flow potential defined as :

$$g_{WC}(\boldsymbol{\sigma}) = J_2(\boldsymbol{\sigma}) + \frac{1}{3} I_1(\boldsymbol{\sigma}) tan(\psi_{WC}) \quad (8)$$

where ψ_{WC} is the dilatation angle. In this paper an associate flow rule is considered, i.e. $\psi_{WC} = \phi_{WC}$.

In the Drucker Prager model, the hardening parameters and yield stress must be determined from a stress-plastic strain curve obtained in monotonic uniaxial compression test. It is interesting to note that under this loading condition, the yield function is identical for both elastoplastic models:

$$f(\boldsymbol{\sigma}, p) = \left|-\sigma_{comp}\right| - R - Y(p) \tag{9}$$

as well as the cumulated plastic strain p computed as follows (see the proof in **Appendix A**):

$$p = \int_0^t \left|-\dot{\varepsilon}_{comp}^{p}\right| dt \tag{10}$$

where $\sigma_{comp} > 0$ and the $\dot{\varepsilon}_{comp}^{p} > 0$ are the normal stress and plastic strain rate in the direction of the compression.

In the following of this study, the von Mises criterion for both phases will be used in the development of this microstructural model. The results of the model will be compared to those calculated from the von Mises and Drucker-Prager criteria applied respectively to the Co and WC behaviours in Subsection 5.4.

2.3 Interfaces

In the composite, two types of interfaces can be observed: WC/Co and WC/WC. In simulations dealing with the behaviour of composites at the microstructure scale, the WC/Co interfaces are represented geometrically. These interfaces are considered as a perfect contact because of the good adhesion between these two phases [24, 25]. This good adhesion can be justified during sintering by a low interfacial energy which leads to an excellent wetting of the cobalt on the WC grains [41]. Regarding WC/WC interfaces, Csanadi et *al.* [42] concluded from micro-bending tests that their bending strength is generally lower than that of the WC grains. Sometimes, these interfaces are represented geometrically in some models but there are considered generally as perfect [24–26]. Their elasto-plastic models, like those presented in Subsection 2.2, are dedicated to polycrystalline materials. Therefore, the influences of grain boundaries are implicitly included in the parameters of these models. The WC/WC interfaces that will be represented in the present work are also considered as perfect.

3. Creation of the microstructure

Simulations are based on a geometrical representation of the microstructure. However, various complex geometries of the WC-Co microstructure are represented in the literature. In several investigations lead by Sadowski et *al.*[22, 32], the composite consists of polygonal WC grains surrounded by a thin layer of cobalt. Faksa et *al.* [26] have also adopted this description in part of their work, which is named "Co-matrix model". Nevertheless, in most representations of the WC-Co microstructure, the WC grains are in contact to form a WC skeleton with WC/WC interfaces that are

excluded in the “Co-matrix model”. The presence of such skeleton was first formulated by Dawihl and Hinnüber [43], observing that the samples maintained their shape after the cobalt had been attacked by boiling HCl. The existence of this skeleton, if any, is conditioned by the cobalt content. However, the percentage of cobalt above which the skeleton is no longer obtained is not well defined. For instance, Exner [3] fixed that limit to 30 wt.%Co while it is about of 11 wt.%Co for Dawihl and Hinnüber [43]. In 2D observations, the cobalt phase seems to be isolated in small areas, especially when the weight percentage of Co is low. Faksa et *al.* [26] also adopted this description which is named "WC-matrix model". According to the results of their research, this microstructural description is more appropriate to represent the elastoplastic behaviour of the composite. However, the hypothesis of an isolated Co phase is no longer necessarily true in the case where the weight percentage of Co increases. Some authors have shown continuous Co skeletons on several WC-Co grades in 3D space [44]. In addition, the distribution of cobalt in the WC-Co composite is not uniform. List et *al.* [45] observed, on the rake face of an uncoated carbide insert (geometry type K4, Sandvik) H13A grade (K20, 6%Co), based on a SEM images, some areas rich in cobalt and others in carbide grains.

Due to the complexity of the WC-Co microstructure, most microstructural simulations in the literature generally use a 2D geometric representation of the microstructure generated from microscopic images. For example, Zhu et *al.* [31] have structured this process in their research in six steps: noise reduction, image binarization, WC grain segmentation, WC grain boundary definition, WC grain boundary vectorization and meshing. Recently, Jiménez-Piqué et *al.* [44] have reconstructed a 3D microstructure from a sequence of images obtained by FIB (Focused Ion Beam Tomography). However, these studies are limited by the number of micrographs and obtaining them is a long process. Alternatives are also proposed in the literature where an idealized WC-Co microstructure is rapidly generated from an algorithm for a given wt.% of Co. For example Park et *al.* [38] proposed an algorithm to build a 2D WC-Co microstructure. In their work, a single WC grain is defined by a quadrangle controlled by four parameters: a centroid, a major axis, a minor axis and the orientation angle measured between a major axis and a horizontal reference line. The values of these parameters are defined from statistical distributions determined on real microstructures. The quadrangles are randomly distributed to generate a WC skeleton. The voids between the WC grains are filled by the Co phase. Kayser et *al.* [46] used truncated prisms for the WC grains and generated a 2D microstructure which is extruded in the third direction.

In the present paper, 2D square microstructures have been created in Matlab using the algorithm proposed by Tkalich et *al.* [25]. The microstructures are generated from the Voronoi cell pattern. Then each cell is divided into two parts by a line. Each part of the cell contains either the WC phase or the Co binder. The temporary crossing point of this line is randomly placed on an edge of the cell. The line makes a randomly imposed angle α with the horizontal in the interval $[0; \pi]$. Then, the shortest

distance between the farthest cell vertex and the line is iteratively calculated such that the predefined surface fraction of the binder phase is reached with an accuracy of more than 98%.

Finally, RVE is extruded to over 1/10 of its lateral length in the third direction as in [47] to perform a 3D computation (see Figure 4). This algorithm makes it possible to rapidly generate a large number of idealized microstructures (or RVE) with different Co contents to analyse its effect on the elasto-plastic behaviour of the composite. Nevertheless, it is necessary to define a minimum number of cells to generate RVEs that will allow to represent the elasto-plastic behaviour of the WC/Co with a good accurate. This cell number is studied in following section.

4. RVE determination

In the literature, the RVE is often defined by the number of WC grains, although their behaviour is that of a polycrystalline WC in the numerical simulations. The number of WC grains and Voronoi cells are identical and controls indirectly the distribution of the cobalt phase. Thus, a large number of WC grains leads to a more homogeneous distribution and smaller islets of cobalt in the microstructure, as shown in Figure 5. In this work, 8 groups of microstructures comprising 5, 50, 100, 150, 200, 250, 275, 300 WC grains are studied for composites of WC-6wt.%Co and WC-20wt.%Co. These two compositions have been chosen to determine an RVE covering a wide range of cobalt content used in cutting tools. For each group, 4 different microstructures have been generated. For all microstructures, simulations have been performed using the finite element method implemented in the ABAQUS Software [37]. Each RVE is subject to kinematic boundary conditions showed in Figure 6 to simulate a uniaxial compression test. This test allows the comparison between the results of the simulation and the experimental data in the literature. As shown in Figure 6, at the left, on the bottom and at the back of the sides of the microstructure, displacements are fixed in the x, y and z directions, respectively. On the upper side (at the left side), a negative displacement $-u_y$ $(-u_x)$ is imposed to performed uniaxial compression in the y (and x) directions. The remaining sides, a relationship between nodes could be applied to impose straight sides. However, Sadowski et *al.* [22] compared this solution with that of free sides and obtained the same results. In the present study, these sides are free. The element type used is a linear prismatic element C3D6 with 6 nodes. A suitable mesh size has been selected from convergence studies for each RVE. For illustrative purposes, Figure 7 shows the normalized Young's modulus and dissipated plastic energy computed with different mesh sizes on RVE of 275 grains. The tested element sizes are 0.042, 0.031, 0.012, 0.007 and 0.005 of the RVE size corresponding to 3595, 4868, 35280, 65631 and 101418 elements. In the following of this study, the third mesh size has been selected.

The criteria to determine the RVE are partly inspired by those proposed by Chen et *al.* [23]. The first criterion is the ratio E_x/E_y where E_x and E_y are the apparent Young's moduli of each microstructure obtained from simulations of uniaxial compression in the x and y directions, respectively. If this

criterion is close to one, then the microstructures are considered isotropic. In Figure 8, the averages of ratio E_x/E_y for each group of microstructures are plotted as a function of the number of grains. For composites containing 6 wt.%Co, this ratio is approximately equal to 1 with an error of less than 1% regardless the number of grains, whereas for its counterpart containing 20wt.%Co, this error is reached from 100 grains upwards. Moreover, for all groups of microstructures larger than 100 grains, as shown in Figure 8, the dispersion of this criterion in each group is low since its standard deviation is less than 0.01. A low standard deviation means that the apparent properties of the RVE are not affected by different microstructures containing the same number of grains. For microstructures with less than 100 grains, the standard deviation is higher because the distribution of the cobalt phase is very heterogeneous.

The second criterion is defined as the ratio E_i/E_{300}, where E_i and E_{300} are the mean Young's moduli of the microstructure groups containing i and 300 grains, respectively. Microstructures composed of 300 grains are taken as a reference since they have the largest number of grains in this study. Moreover, it is likely that their apparent mean Young's modulus already converges to the effective Young's modulus of the composite as observed by Chen et *al.* in [23]. The E_{300} values for the WC-6wt.%Co and WC-20wt.%Co composites are 623 and 480 GPa, respectively. Figure 9 shows a variation of the ratio E_i/E_{300} and its standard deviation as a function of the number of grains. As for the previous criterion, from 100 grains upwards, all ratios E_i/E_{300} are close to 1 with an error of less than 1% and a standard deviation of less than 0.01. In other words, the ratio converges quickly, and the apparent Young's modulus of the microstructures is close to the values of E_{300}. The same trends are also observed for Poisson's ratio and thermal expansion. However, as mentioned by Chen et *al.* in reference [23], the RVE defined with the elastic phases cannot be sufficient to perform a plastic study of the composite due to the development of the overall non-linearity of the material. It is therefore necessary to continue this study by selecting a criterion for the determination of the RVE taking into account the plastic behaviour of each phase.

The third criterion is the P/U ratio where P and U are respectively the average plastic energy dissipated and the external work, for a total deformation of 2% obtained by simulating a uniaxial compression test. Figure 10 shows the mean value of the P/U ratio and its standard deviation as a function of number of grains for the two cobalt grades. The P/U ratio begins to converge towards the value of about 0.46 and 0.38 from 200 grains for microstructures containing 6 and 20 wt.% of cobalt, respectively, with standard deviations less than 0.01. As suspected, the number of grains where this criterion converges is greater than that observed in the elasticity studies.

Note that a final criterion often used in the literature to determine an RVE can also be applied. This is the Hill's criterion, which is independent of the mechanical behaviour under consideration. According to Chen et *al.* [23], this criterion can be written as follows :

$$\psi = \max\left(\frac{\langle\sigma\rangle:\langle\varepsilon\rangle}{\langle\sigma:\varepsilon\rangle}, \frac{\langle\sigma:\varepsilon\rangle}{\langle\sigma\rangle:\langle\varepsilon\rangle}\right) \quad (11)$$

If this criterion tends towards 1, then the RVE is correctly defined. Figure 11 shows the mean value of ψ and its standard deviation as a function of the number of grains. ψ is equal to 1 for the composite WC-6wt.%Co while its counterpart with WC-20wt.%Co decreases to converge towards 1.16 from 250 grains. For microstructures larger than 250 grains, the standard deviations of ψ for both grades are less than 0.01.

According to the different criteria defined above, an RVE with a number of grain greater than 250 can be selected with confidence. A RVE with 275 WC grains is selected in the following. This number is comparable to the one found by Chen et *al.* Sadowski et *al.* [22] for a RVE with a size of 40x40 μm and an average tungsten carbide grain size of 2.35 μm (i.e. 290 WC grains for a cobalt-free composite).

5. Results and discussion

The RVE being defined, the numerical model is tested to validate its ability to reproduce the elastic and elasto-plastic experimental behaviours of the composite.

5.1 Elastic behaviour validation of the model

The validation of the elastic behaviour of the model consists in predicting the Young's moduli of composites containing 6, 10, 12 and 20 wt.% Co (0.9, 0.83, 0.8 and 0.675 WC volume fraction respectively) and comparing them with experimental data obtained in the literature [48–51], see Figure 12.

For each composite, four quasi-realistic microstructures have been generated. The calculated maximum deviation is less than 0.6%. Consequently, the error bar corresponding to the dispersion of the results of the realizations is not visible on Figure 12. A good agreement between the calculated and measured Young's moduli is obtained, in particular with the data provided by Schwartzkopf and Kieffer [48]. The numerical results are included in the scatter of the experimental data set which is of the order of about 50 GPa for the same cobalt content. The increase in Young's modulus as a function of WC volume fraction is also well reproduced. This test was often used in the literature by Jaensson and Sundström [19], and Tkalich et *al.* [24] to evaluate the robustness of the model.

5.2 Elastoplastic behaviour validation of the model at room temperature

The second validation is the reproduction of the stress-strain curve measured by Teppernegg et *al.* [30] up to a total strain of 2% for a WC-6wt.%Co composite in uniaxial compression at room temperature, see Figure 13. In Figure 13, the simulated stress-strain curves with the hardening parameters taken from the work of Tkalich et *al.* [24] ($Q_{WC} = 3000\ MPa$ and $b_{WC} = 10$) reproduce the experimental

data up to 0.5% strain. Beyond this deformation, the hardening of the composite calculated by the model is lower than that observed on the experimental curve. The stress is underestimated up to 33% of the measured value for a 2% deformation. The hardening parameters used do not seem adequate to reproduce the experimental data. However, the stress-strain curves of the composite depend on the WC grain size [40]. The experimental curves measured by Teppernegg et *al.*, used as a reference for this study, were measured on composites with a grain size of about $1\mu m$. Therefore, the hardening parameters Q_{WC} and b_{WC} of the carbide phase must be redefined so that the simulated curve corresponds to that measured on the composite knowing that the elastoplastic behaviour of cobalt is already defined. Although the WC grain size effect on the composite is beyond the scope of the present paper, this one would be considered by Hall-Petch type relationships in the elasto-plastic models [52, 53]. Indeed, this size cannot be considered using the geometry of the microstructure generated in Section 3 because the models are based on the continuum mechanics theory insensitive to the absolute size, [21].

The first parameter Q_{WC} represents the difference between the maximal compressive stress that the WC phase can achieve and its compressive yield stress R_{WC}. If Q_{WC} is zero, the material is perfectly plastic. The second parameter b_{WC} controls the growth rate of the stress in the elastoplastic regime of the WC. These parameters, despite of the presence of the cobalt, seems to have the same influence on the composite behaviour. Indeed, when only Q_{WC} increase up to 6000 MPa with $b_{WC} = 10$, the stress of the composite rises from 3925 MPa to 4200 MPa for strain of 2%, see Figure 13. If b_{WC} is multiplied by 50, the stress increases rapidly. For a strain of 1%, the slope of the curve for $b_{WC} = 500$ is equal to 2520 MPa/% versus 570 MPa/% for $b_{WC} = 10$. The combination $Q_{WC} = 3000\ MPa$ and $b_{WC} = 500$ has been found by trial and error to be in good agreement with the experimental counterpart and will be use in the following of this paper. By comparison with the values of Q_{WC} and b_{WC} proposed by Tkalich et *al.* [24, 25], only the last parameter changes.

In conclusion of this section, the mechanical behaviour of the composite can be represented from these phases and especially from the carbide phase which is fully defined at room temperature. The stress-strain curves of Co and WC are the lower and upper limits, respectively, of the composite behaviour as shown in Figure 14. If both phases are considered elastic, this assumption is valid for deformations of less than 0.4% as shown in the WCECoE curve (WC elastic; Co elastic). In the case where only cobalt has an elasto-plastic behaviour (see the WCECoP (WC elastic; Co plastic) curve in Figure 14) as in the studies of several authors [19, 21, 32, 40], this model is valid up to deformations of 0.6%. Beyond this deformation, the plasticity of the cobalt in the model is no longer sufficient to reproduce the experimental curve of the composite. This observation shared by Faksa et *al.* [26] led the authors to introduce the plasticity of the carbide. Poech et *al.* [21], indicated that it is necessary to take into account the plasticity and/or damage processes in the carbide phase after the initial plasticity of the composite. However, according to the results of Tkalich et *al.* [24], plasticity is activated in the WC

phase well after that of cobalt in the composite due to the lower yield stress of cobalt. This tendency is also observed in the present model because the curve considering the plasticity of the two phases (WC-CoP) merges with the WCECoP curve before a deformation of 0.6%. Finally, the WC-CoP deformation curve reproduces the response of the WC-Co composite under uniaxial compressive loading up to 2% deformation.

5.3 Simulation of the composite at different temperatures

So far, simulations previously carried out have been limited to room temperature. As presented in the introduction, the composite WC-Co used in cutting tools are subjected to different temperatures during machining. Therefore, the effect of temperature must be taken into account in this modelling. The Young's modulus and the thermal expansion of Co and WC are already dependent on temperature as well as the elastoplastic behaviour of the Cobalt phase, see Section 2. In order to complete the present modelling, it is necessary to have compressive stress-strain curves of the WC for different temperatures which are scare in the literature. To overcome this obstacle, a strategy similar to that proposed by Faksa et al. [26] was adopted by reconstructing the WC behaviour from Co and a composite WC-6wt.%Co. For the composite, the compressive stress-strain curves were measured by Teppernegg et *al.* [30] up to 2% strain at temperatures of 25, 200, 400, 600, 800 and 900°C, see Figure 16.

In order to take temperature into account in the plastic regime of the carbide phase, the following modification of the yield criterion was introduced :

$$f_{WC}(\boldsymbol{\sigma}, p, T) = \sigma_{eq} - R_{WC}(T) - \alpha_2(T) Y_{WC}(p) \tag{12}$$

with $R_{wc}(T)$ defined as following :

$$R_{wc}(T) = \alpha_1(T) R_{wc}(T = 25°) \tag{13}$$

$\alpha_1(T)$ and $\alpha_2(T)$ control the temperature dependence of the yield stress $R_{wc}(T)$ and the isotropic hardening of the WC material, respectively. Note that for $T = 25°C$, $\alpha_1 = \alpha_2 = 1$. This modification is valid for both von Mises and Drucker Prager criteria since their compressive stress-strain curves are equivalent changes. The parameters α_1 and α_2 will implicitly include the observed modifications in the behaviour of WC-Co with increasing temperature. Mari [15], this change occurs from 527°C and is explained by an increase in toughness induced by the softening of cobalt under limited plastic deformation. The sliding of WC grain boundaries is one of the mechanisms involving this softening as reported by several authors [15, 54]. Above 827 °C, the behaviour of the composite is entirely plastic.

For the reconstruction of the elasto-plastic behaviour of the WC, the temperature-dependent evolution of one of the parameters will be imposed while the other will be defined from the compressive stress-strain curves of the composite for different temperatures.

$\alpha_1(T)$ has been calculated assuming that the evolution of the ratio $\sigma_{wc-}\ \ (T)/\sigma_{wc-Co}(T = 25°C)$ of the composite is the same as that of the WC material. $\sigma_{wc-Co}(T)$ and $\sigma_{wc-Co}(T = 25°C)$ are the stresses of the composite measured at a given temperature and at room temperature, respectively, for a plastic deformation of 0.2%. This assumption may be rough, but it ensures that the yield stress of WC is always higher than that of the composite. Indeed, as shown in Figure 14, the behaviour of the composite is between that of carbide and cobalt. It allows the cobalt to deform plastically over a wide range of strains before the carbide deformations occur in the composite. $\alpha_2(T)$ have been determined by performing several simulations to reach, by trial and error, a good agreement with the experimental stress-strain curves of the composite, see Figure 16. The values of $\alpha_1(T)$ and $\alpha_2(T)$, shown in Figure 15, decrease gradually as the temperature increases. Nevertheless, their respective evolutions are independent although $\alpha_1(T)$ and $\alpha_2(T)$ are close for 200, 400, 800°C. In other words, the evolution of the yield stress as a function of temperature is not dependent on that of the hardening.

The plastic stress-strain curves of the WC in compression can be plotted for different temperatures as shown in Figure 17 and compared with the results obtained by Faksa et *al.* [26]. Let us recall that these authors determined the behaviour of the WC, with a similar strategy, more precisely, from those of the composite WC-6wt.%Co and a cobalt alloy. The orders of magnitude of the stresses are almost similar, except for the shape of the curves and the yield stress. The shape of the curves in this case is imposed by the relation (4), while those of Faksa et *al.* are obtained directly from the simulation results. The yield stresses of WC obtained by these authors overestimates by 1 GPa those of this paper for temperatures of 25°C, 200°C, 400°C. However, they are almost identical for temperatures above 600°C. It can be noted that the determination of the yield stress of WC is not obvious because according to Csanádi et *al.* [55], the tolerance in its measurement can reach 1 GPa.

As the parameters $\alpha_1(T)$ and $\alpha_2(T)$ are determined from the data of the composite WC-6 wt.%Co, the model is applied to compression tests of a composite WC-10.5wt.%Co measured by Teppernegg et *al.* [30] for different temperatures, see Figure 18. All model parameter values are summarised in Table 1. For temperatures above 600°C, the model overestimates the experimental curves for a strain of 0.25% at T=900°C. On the other hand, for temperatures less than or equal to 600°C, the simulations underestimate the experimental data with a maximum error of 30 % for a strain of 0.3% at T=600°C. Note that the difference between the calculated and measured curves reduces as the temperature decreases. The modelling correctly predict the measured stress-strain curves, especially for strains greater than 1% (except for the one obtained at 900°C). After 800°C, the elasto-plastic laws used in the present modelling seem less appropriate as the material becomes more sensitive to strain rate (Smith and Wood 1968). Teppernegg's et al. (Teppernegg et al. 2016) obtained experimental data with an imposed strain rate of 5.10^(-3) s^(-1) corresponding to that encountered in creep tests (Sakuma and Hondo 1992). For high temperatures, visco-plastic models would be more suitable to reproduce the behaviour of carbide and cobalt phases.

5.4 Comparison between the models using von Mises and Drucker Prager criteria for WC

So far, simulations presented above have been performed with the von Mises criterion applied to the carbide phase. The hardening parameters $Q_{WC} = 3000\ MPa$ and $b_{WC} = 500$ as well as the parameters $\alpha_1(T)$ and $\alpha_2(T)$ found previously have been also applied for the Drucker Prager criterion. Figures 19 and 20 show a comparison between these two criteria on the stress-strain curves computed at different temperatures for the carbide grades WC-6wt.%Co and WC-10.5wt.%Co, respectively. The curves computed with both criteria for the WC-6wt.%Co composite are almost identical, when the behaviour of the WC phase is determined with the von Mises criterion, the average stress tensor, shown by the relation (14), is close to a state of uniaxial compressive stress.

$$\boldsymbol{\sigma} = \begin{pmatrix} 241 & -4.4 & 0.9 \\ -4.4 & -6106 & -1.3 \\ 0.9 & -1.3 & 278 \end{pmatrix} MPa \tag{14}$$

This tensor has been computed at room temperature and for a strain of 2%. The same case for the stress tensor was computed with the Drucker Prager criterion, see relation (15).

$$\boldsymbol{\sigma} = \begin{pmatrix} 150 & -5.9 & 0.7 \\ -5.9 & -5946 & -0.9 \\ 0.7 & -0.9 & 170 \end{pmatrix} MPa \tag{15}$$

As mentioned in Section 2.2.2 and **Appendix A**, for this mechanical loading, the two models are equivalent explaining the curves superpositions of Figure 19.

However, the stress states calculated at each integration point are locally different due to the complex shape of the WC phase and can be represented by points in a diagram $p - J2$ in order to analyse their dispersion. This type of diagram also used by Tkalich *et al.* [25] is plotted for both criteria in Figures 21(a) and (b) at room temperature for a total strain of 2%. Most of these points are concentrated in the vicinity of the bold red line which represents the load path for a uniaxial compression. The green and blue lines symbolize the initial and maximum yield stresses, respectively. In Figure 21(b), these last two lines are tilted in the case of the Drucker Prager model because of its dependence on pressure. For this model, the diagram clearly shows the difference between the compressive and tensile yield stress with a shorter load path for the tensile depicted by the blue line. Another difference between these two criteria is that certain stress states may exist in one of these two models and not in the other. For example, in Drucker Prager's model for high pressures, some points are above the maximum yield stress of the Mises model, see Figure 21(a). The opposite can be observed for low pressures, where some points calculated with the von Mises criterion are above the maximum yield stress of the Drucker Prager criterion. However, this concerns only a few points and has no impact on the stress-strain curves of this composite in compression as shown in Figure 19.

As the cobalt content increases, the shape of the WC phase becomes more complex and involves more varied stress states in the microstructure. In the case of the composite WC-10.5wt.%Co, the dispersion of the points is greater with an increase in the number of areas in the microstructure with low plasticity in the WC as shown Figures 21(c) and d. For the Drucker Prager model, in Figure 21(d) a shift of most of the points from the compression path towards low pressures in the diagram $p - J_2$, is also observed. These data have been calculated for both criteria at room temperature for a total strain of 2%. In this case, the average stress state gets away from a uniaxial compressive mechanical load and therefore these models are no longer equivalent. That is why there is a slight difference between the curves in Figure 20 calculated according to these two criteria. The discussions and comments written in the previous section between the experimental data and the results of the von Mises model can be applied to the Drucker Prager model.

For future simulations at the microstructural scale, the Drucker Prager criterion is better suited to represent the behaviour of the WC phase because it can simulate the difference between the tension and compression behaviours observed in the composite.

6. Conclusions and Perspectives

In this paper, a microstructure scale modelling has been proposed to simulate the elastoplastic behaviour of the WC-Co composite with different contents of cobalt and various temperatures from 25 to 900 °C.

The elastoplastic behaviour of each phase has been identified from the literature. The cobalt has been modelled with the von Mises criterion for its plastic behaviour. This criterion and the Drucker Prager one have been used in the first instance for the tungsten carbide phase at room temperature. Although its behaviour is often considered elastic, it has been extended to the field of plasticity to simulate the compression of the composite for strains greater than 0.6%. The properties at the WC-WC and WC-Co interfaces as well as the WC grain size effect have not been considered. Thereafter, realistic microstructures have been generated by an algorithm inspired from the work of Tkalich et al. [25] to control the grain number of WC and the cobalt content.

Then, a study has been led to determine the WC grain minimum number in a representative volume element to reproduce the macroscopic behaviour of the composite in compression. The convergence of the criteria as the isotropy of the elastic behaviour, the Young's modulus, the ratio between the dissipated plastic energy and the external work and the Hill's criterion have been achieved for microstructures which the number of WC grain is larger than 250.

In the following of this study, the hardening parameter of plastic behaviour models for the carbide phase have been determined $Q_{WC} = 3000\ MPa$ and $b_{WC} = 500$ from the uniaxial compression tests performed on a grade WC-6wt.%Co at room temperature. Then, the yield criterion has been extended

to different temperatures by the introduction of two functions $\alpha_1(T)$ and $\alpha_2(T)$. These two parameters represent the dependence of the yield stress and hardening on temperature, respectively. These functions have been determined with a microstructure of 275 grains from the elastoplastic behaviour of the cobalt and composite WC-6wt.%Co for a temperature range of [20-900°C] with the von Mises model.

Simulations have been performed to predict the stress-strain curves in compression of the composite WC-10.5wt.%Co compared with experimental data taken from the work of Teppernegg et *al.* [30]. A good agreement was observed for all temperatures for a strain larger than 1% excepted for 900°C. Before this strain, the model overestimates and underestimates the experimental curves for temperatures larger and lower than 600°C, respectively.

A comparison between the von Mises and Drucker Prager criteria applied to the carbide phase have been also discussed. Both models lead to equivalent results in uniaxial compression. Nevertheless, the local stress states between these approaches become different when the cobalt content increases. However, it is recommended to use Drucker Prager criterion because it can reproduce the difference between yield stress in traction and compression observed in the composite.

The model presented in this work assumes that the decrease in the stress rate for large deformations is only due to plastic deformations. Possible extensions and improvements can be proposed in forthcoming work, such as considering the damage and the visco-plastic behaviour of the composite phases. In addition, the used plastic models neglect the WC and Co grain size and their orientation. It would be interesting to use the crystal plasticity for both phases for a more accurate description of the composite behaviour.

Appendix A. Proof of the equivalence of the von Mises and Drucker Prager elasto-plastic models under a compression loading

The following appendix shows that the plastic stress-strain curves of the uniaxial compression test obtained in the compression axis are equivalent for the Mises and Drucker Prager models if $\phi_{WC} = \psi_{WC} = 45°$. Only the quantities useful for this proof are defined. For more information on undefined quantities, please refer to Section 2. The MS and DP indices attached to the quantities refer to the von Mises and Drucker Prager models.

In the uniaxial compressive test, Cauchy stress tensor is written as follow :

$$\boldsymbol{\sigma} = \begin{bmatrix} -\sigma_{com} & 0 & 0 \\ 0 & 0 & 0 \\ 0 & 0 & 0 \end{bmatrix} \tag{A.1}$$

with $\sigma_{com} > 0$, the magnitude of the stress in the direction of compression.

The yield surface for both models is

$$f_{WC}(\boldsymbol{\sigma}, p) = \sigma_{eq} - (R_{WC} + Y_{WC}(p)) \tag{A.2}$$

In the von Mises model, the equivalent stress is $\sigma_{eqMS} = J_2(\boldsymbol{\sigma})$. For the stress state of (A.1), $\sigma_{eqMS} = \sigma_{com}$. In the Drucker Prager model, the equivalent stress is $\sigma_{eqDP} = \frac{J_2(\boldsymbol{\sigma}) + I_1(\boldsymbol{\sigma})\tan(\phi_{WC})/3}{1 - \tan(\phi_{WC})/3}$ with $\phi_{WC} = 45°$. For the stress state of (A.1), the equivalent stress is also the one computed with the Mises model, i.e. $\sigma_{eqDP} = \sigma_{com}$.

In relation (A.2), the accumulated plastic strain p, for the von Mises model is defined as follow :

$$p_{MS} = \int_0^t \dot{\varepsilon}_{eqMS}\, dt = \int_0^t \sqrt{\frac{2}{3}\dot{\boldsymbol{\varepsilon}}^{\boldsymbol{P}}_{\boldsymbol{MS}} : \dot{\boldsymbol{\varepsilon}}^{\boldsymbol{P}}_{\boldsymbol{MS}}}\, dt \tag{A.3}$$

with plastic strain rate equivalent $\dot{\varepsilon}_{eq}$ which is computed from the plastic strain rate tensor $\dot{\boldsymbol{\varepsilon}}^{\boldsymbol{P}}_{\boldsymbol{MS}}$ computed from the associate flow rule :

$$\dot{\boldsymbol{\varepsilon}}^{\boldsymbol{P}}_{\boldsymbol{MS}} = \dot{\lambda}\frac{\partial f_i}{\partial \boldsymbol{\sigma}} \tag{A.4}$$

In the case of the stress state given in (A.1), the plastic strain is :

$$\dot{\boldsymbol{\varepsilon}}^{\boldsymbol{P}}_{\boldsymbol{MS}} = -\dot{\varepsilon}_{com}\begin{pmatrix} 1 & 0 & 0 \\ 0 & -\frac{1}{2} & 0 \\ 0 & 0 & -\frac{1}{2} \end{pmatrix} \tag{A.5}$$

with $\dot{\varepsilon}_{com} > 0$ the magnitude of the strain rate plastic deformation in the compressive direction.

590 Therefore, the plastic strain rate equivalent is $\dot{\varepsilon}_{eqMS} = \dot{\varepsilon}_{com} > 0$.

591 For the Drucker Prager model, the accumulated plastic strain is defined as :

592 $$p_{DP} = \int_0^t \dot{\varepsilon}_{eqDP}\, dt = \int_0^t \frac{\boldsymbol{\sigma} : \dot{\boldsymbol{\varepsilon}}_{\boldsymbol{DP}}^{\boldsymbol{P}}}{\sigma_{eqDP}} dt \quad \text{(A.6)}$$

593 With equivalent plastic strain rate $\dot{\varepsilon}_{eqDP}$ which is computed from the plastic strain rate tensor $\dot{\boldsymbol{\varepsilon}}_{\boldsymbol{DP}}^{\boldsymbol{P}}$
594 obtained from the flow rule :

595 $$\dot{\boldsymbol{\varepsilon}}_{\boldsymbol{DP}}^{\boldsymbol{P}} = \dot{\lambda} \frac{\partial g_{WC}}{\partial \boldsymbol{\sigma}} \quad \text{(A.7)}$$

596 The flow potential for $\psi_{WC} = 45°$ is :

597 $$g_{WC}(\boldsymbol{\sigma}) = J_2(\boldsymbol{\sigma}) + \frac{1}{3} I_1(\boldsymbol{\sigma}) tan(\psi_{WC}) \quad \text{(A.8)}$$

598 In the case of the stress state given in (A.1), the plastic strain is :

599 $$\dot{\boldsymbol{\varepsilon}}_{\boldsymbol{DP}}^{\boldsymbol{P}} = -\dot{\varepsilon}_{com} \begin{pmatrix} 1 & 0 & 0 \\ 0 & -\frac{15}{12} & 0 \\ 0 & 0 & -\frac{15}{12} \end{pmatrix} \quad \text{(A.9)}$$

600 Therefore, the equivalent plastic strain rate is $\dot{\varepsilon}_{eqDP} = \dot{\varepsilon}_{com}$ which is identical to the one computed
601 with the von Mises model.

602 To conclude, for both models, the accumulated plastic strain is

603 $$p = \int_0^t \dot{\varepsilon}_{com}\, dt = \varepsilon_{com} \quad \text{(A.10)}$$

604 as well as the yield surfaces are the same. Consequently, the curves (σ_{comp},ε_{com}) plotted for these
605 models are equivalent.

606 # Acknowledgment

607 The author wishes to thank the French ministry of higher education, research and innovation for
608 financial support.

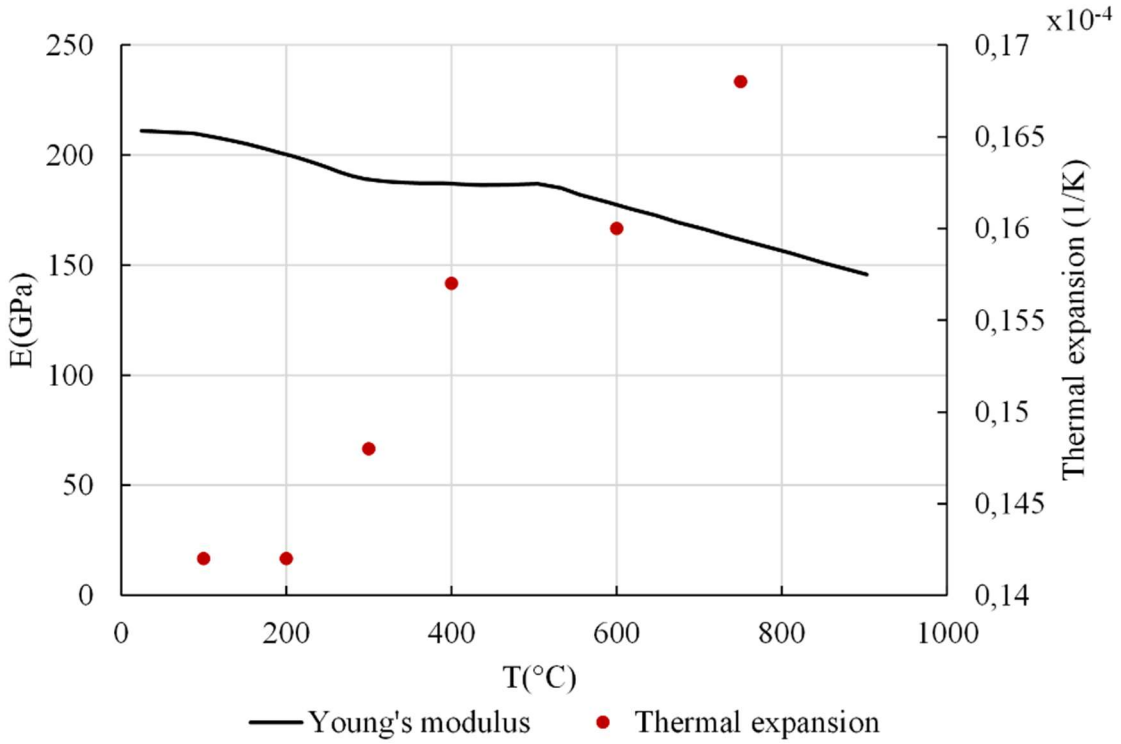

609

610 Figure 1. Young's modulus and thermal expansion used for the Co-phase as a function of temperature,
611 [28, 29].

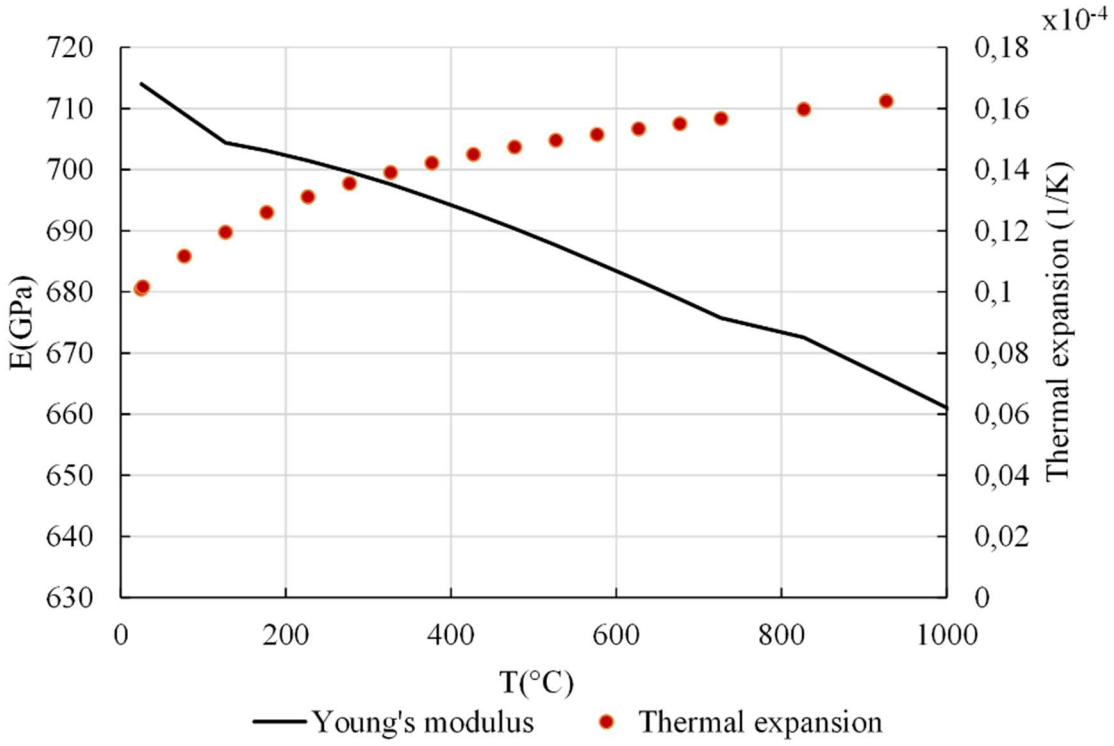

612

613 Figure 2. Young's modulus and thermal expansion used for the WC-phase as a function of
614 temperature, [21, 33, 57].

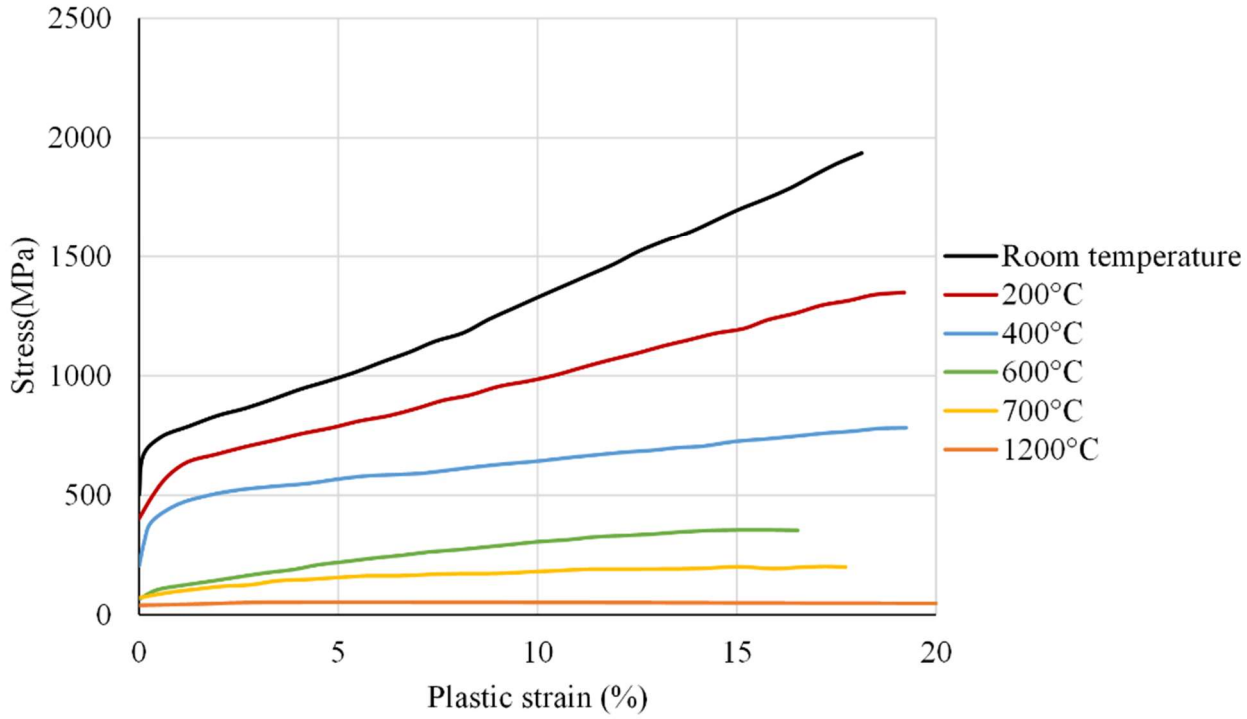

615

616 Figure 3. Stress-plastic strain curves of the Co-phase in uniaxial compression for different
617 temperatures, [38].

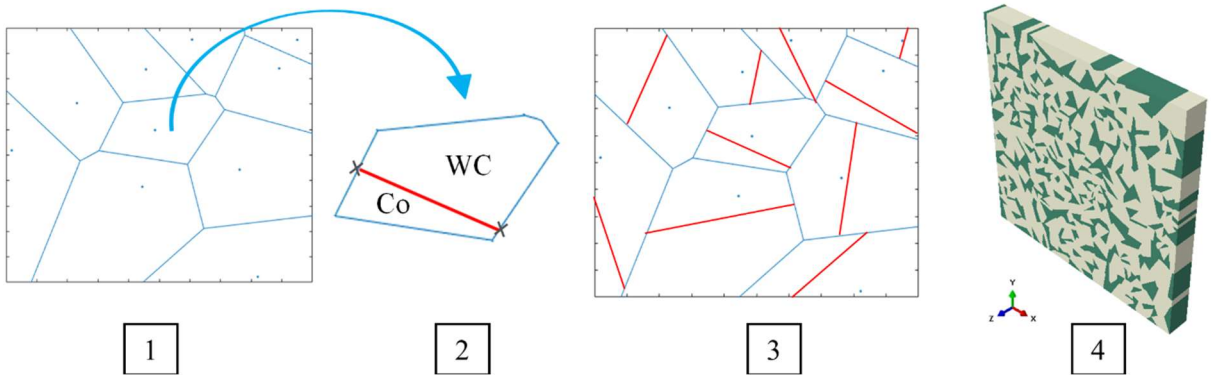

618

619 Figure 4. (1) Construction of the Voronoi cells based on random point distribution. (2) Partition of
620 each cell into two phases. (3) Obtained 2D microstructure. (4) Extrusion of the microstructure in the *z*
621 direction.

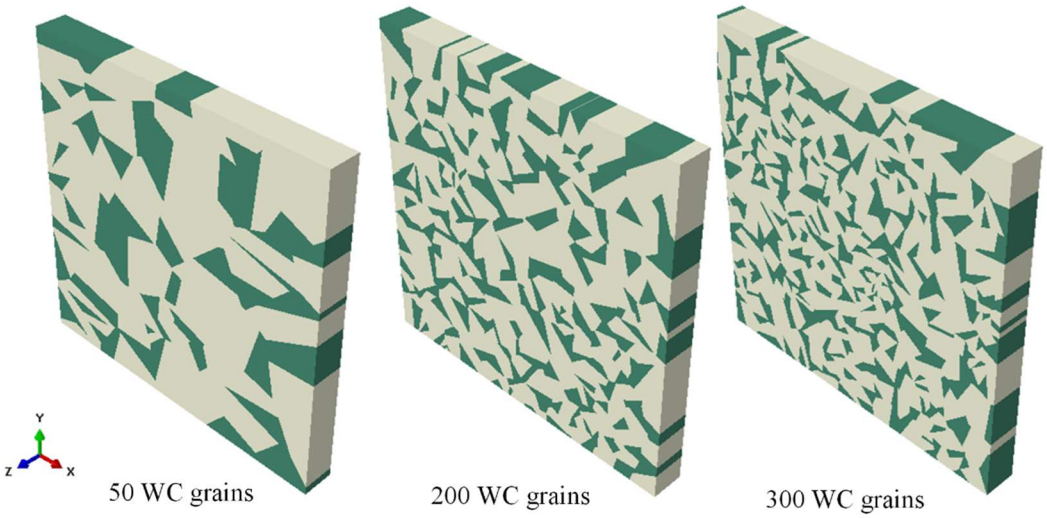

622

623 Figure 5. Representative elementary volumes with different numbers of WC grains (WC-20wt.%Co).

624

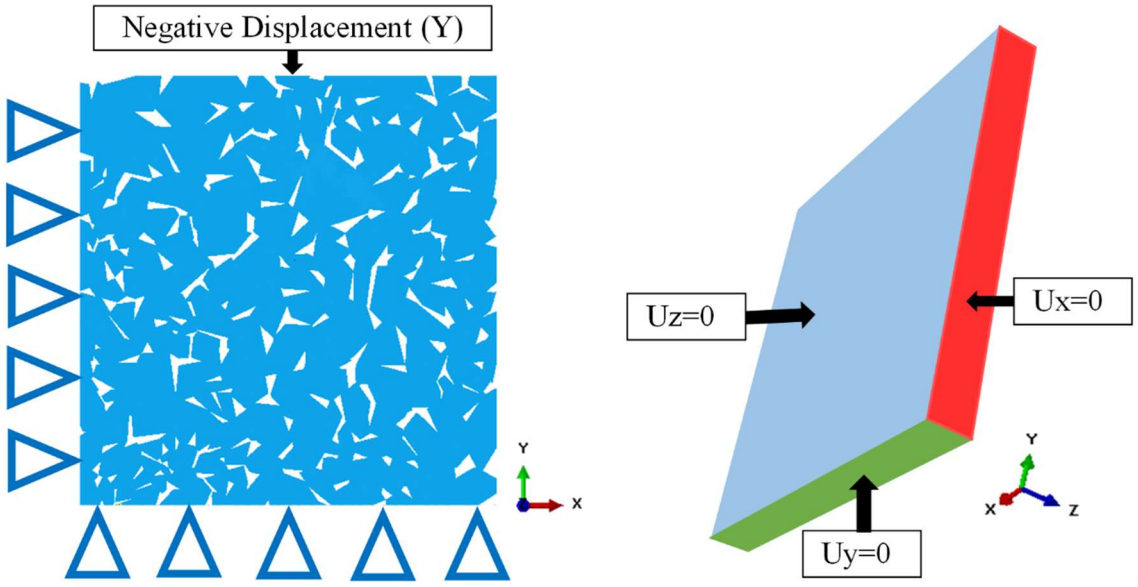

625

626 Figure 6. Boundary conditions applied on the RVE. *Ux*, *Uy* and *Uz* are the displacements in *x*, *y* and *z*
627 directions, respectively.

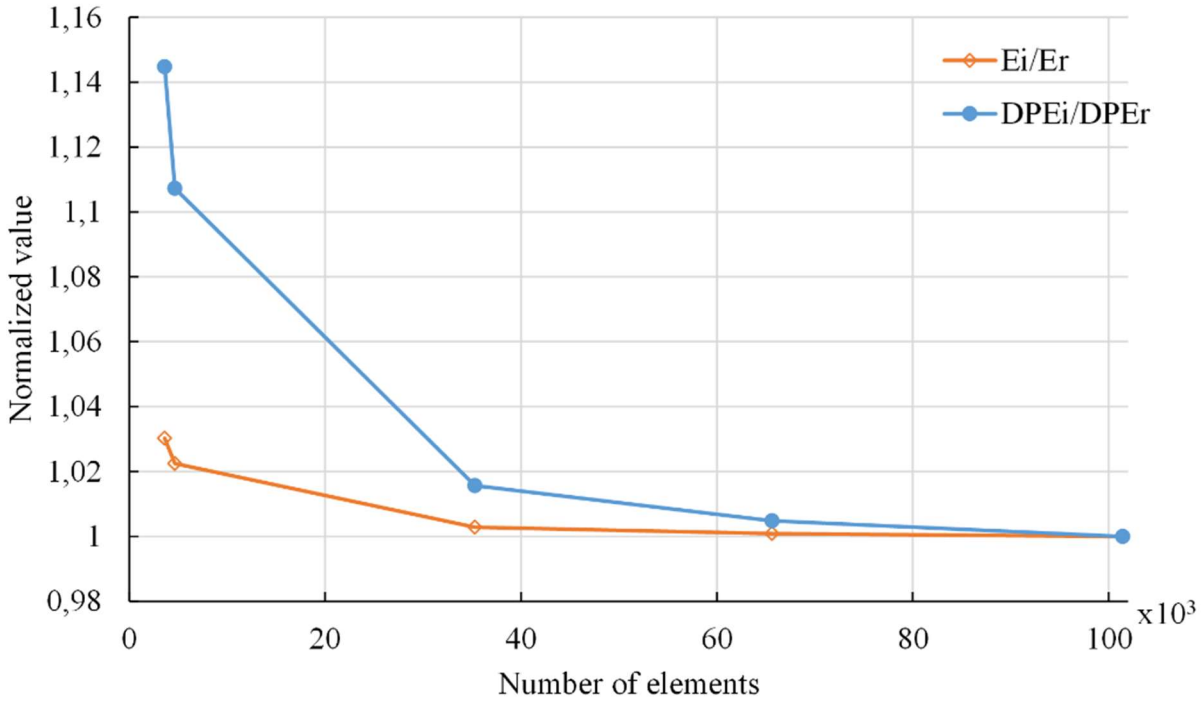

628

629 Figure 7. Influence of the number of elements "i" on the ratios E_i/E_r and DPE_i/DPE_r. The couples
630 E_r, E_r and DPE_r, DPE_r are the Young's moduli and dissipated plastic energies. The r index means
631 that quantities are computed for 100,000 elements.

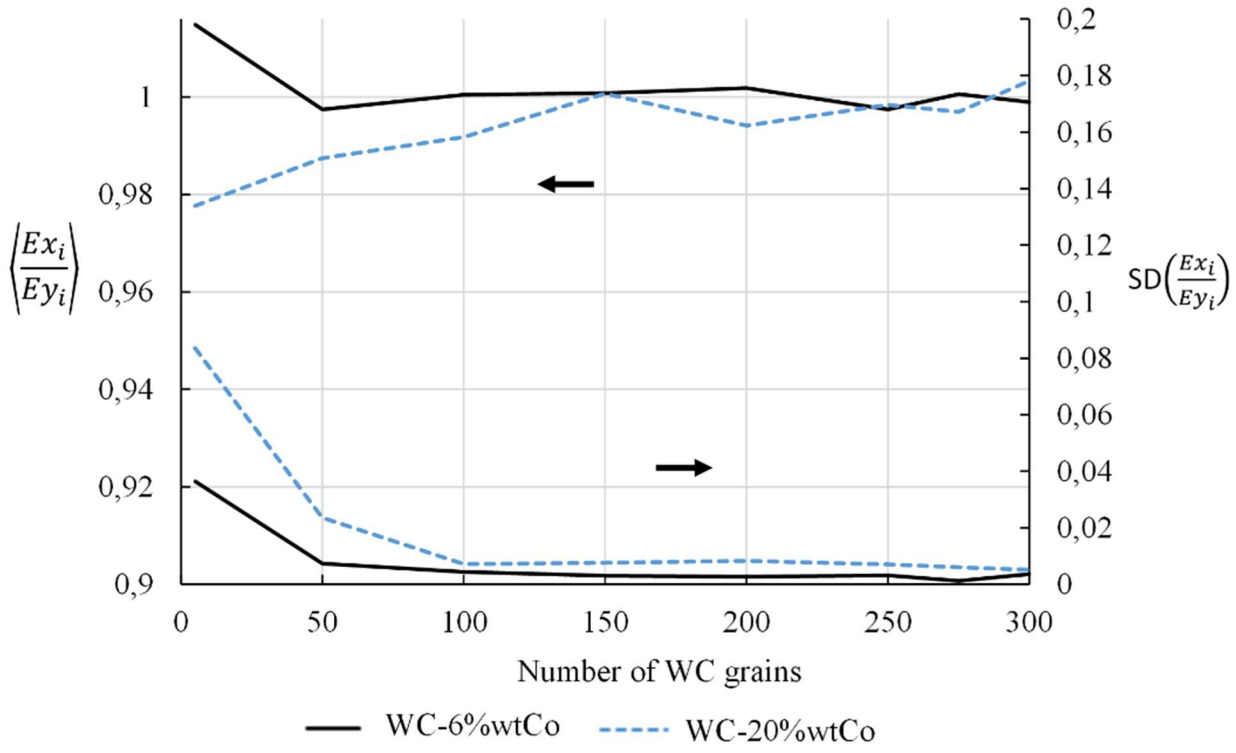

632

633 Figure 8. Evolution of the mean (<>) and standard deviation (SD) of the ratio E_{xi}/E_{yi} as a function of
634 the WC grains number "*i*". E_{xi} and E_{yi} are the Young's moduli computed in the *x* and *y* directions for
635 "*i*" elements, respectively.

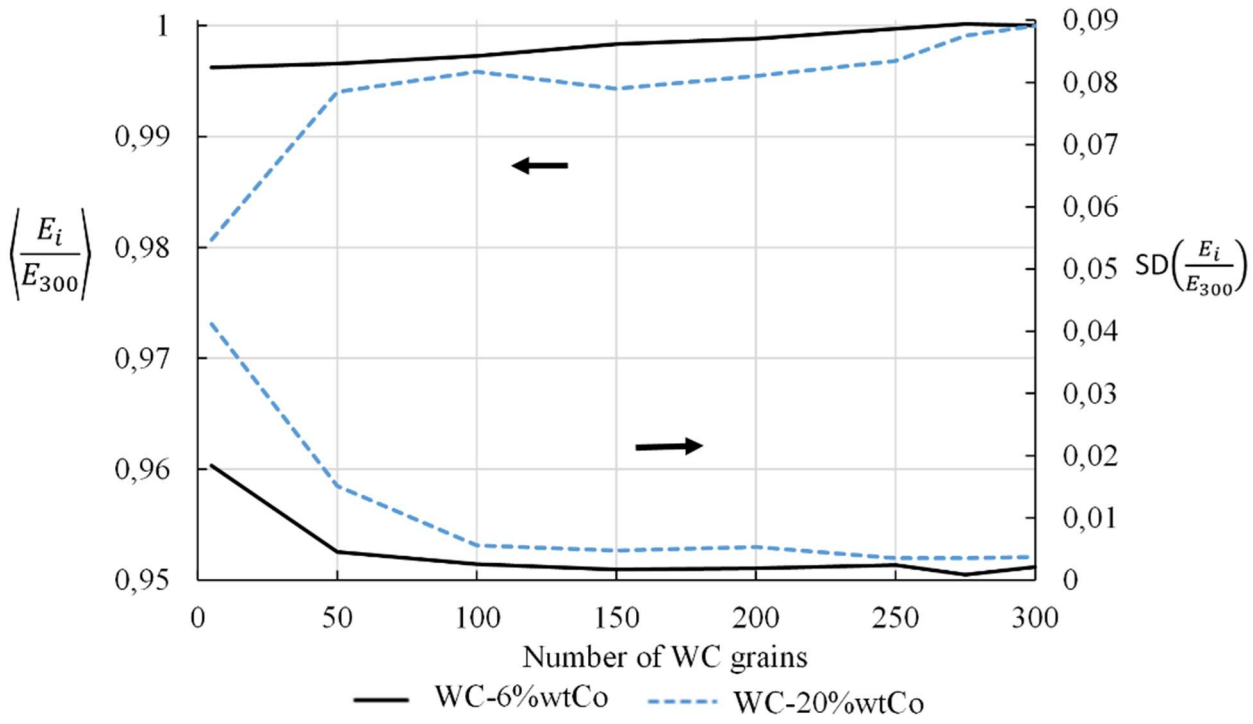

636

637 Figure 9. Evolution of the mean (<>) and standard deviation (SD) of the ratio E_i/E_{300} as a function of
638 number of WC grains "*i*". E_i is the Young's modulus computed for i grains while E_{300} is the mean
639 Young's modulus computed for 300 grains.

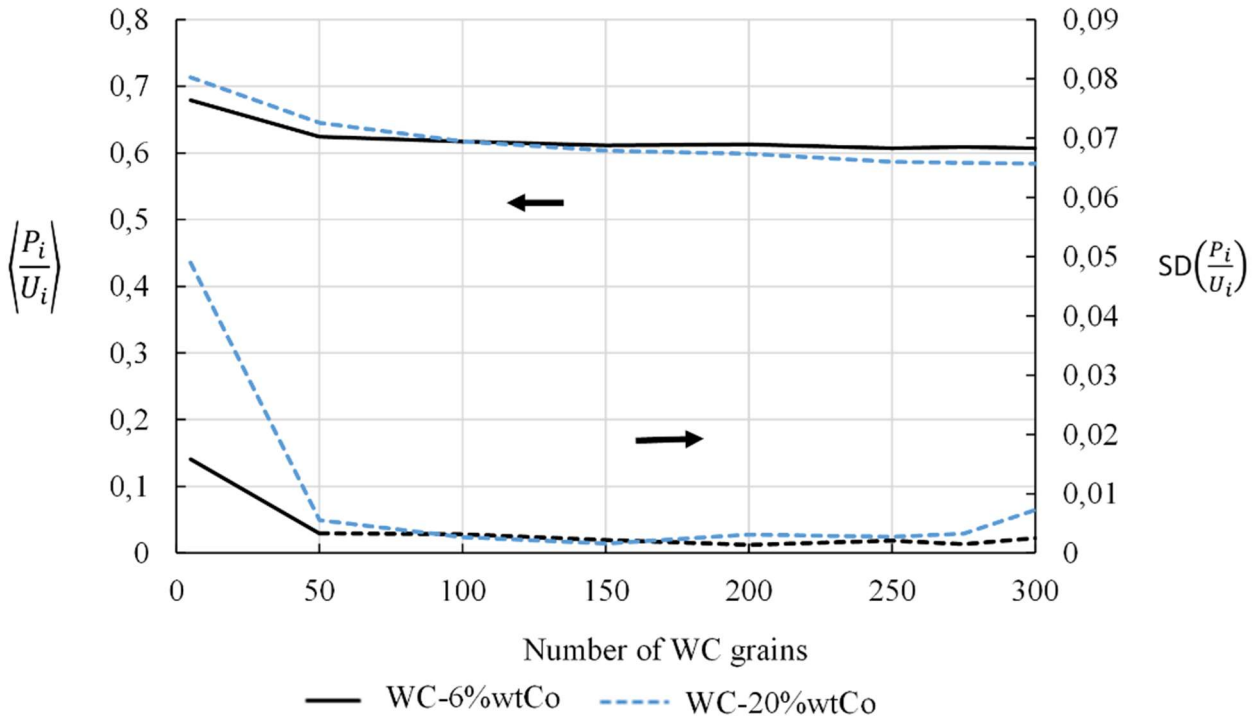

Figure 10. Evolution of the mean (<>) and standard deviation (SD) of the ratio P_i/U_i as a function of the number of grains "*i*". P_i and U_i are the dissipated plastic energy and the external work, respectively.

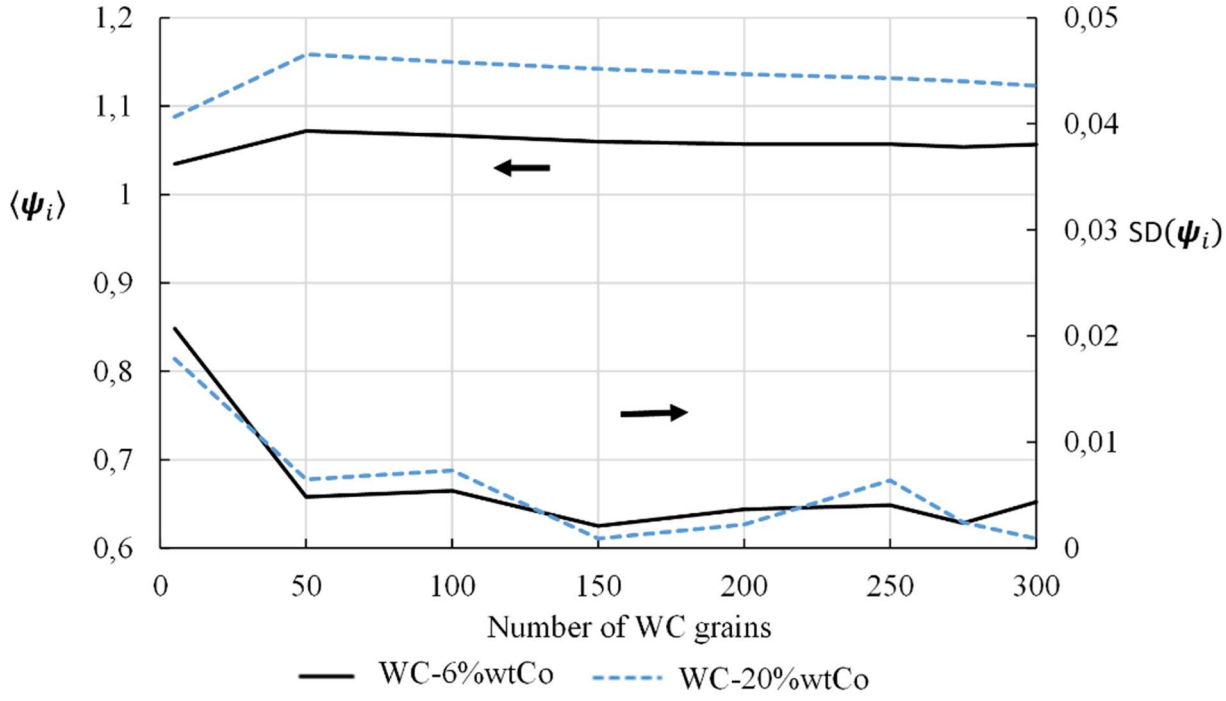

Figure 11. Evolution of the mean (<>) and standard deviation (SD) of Hill criteria ψ_i as a function of WC grains "i".

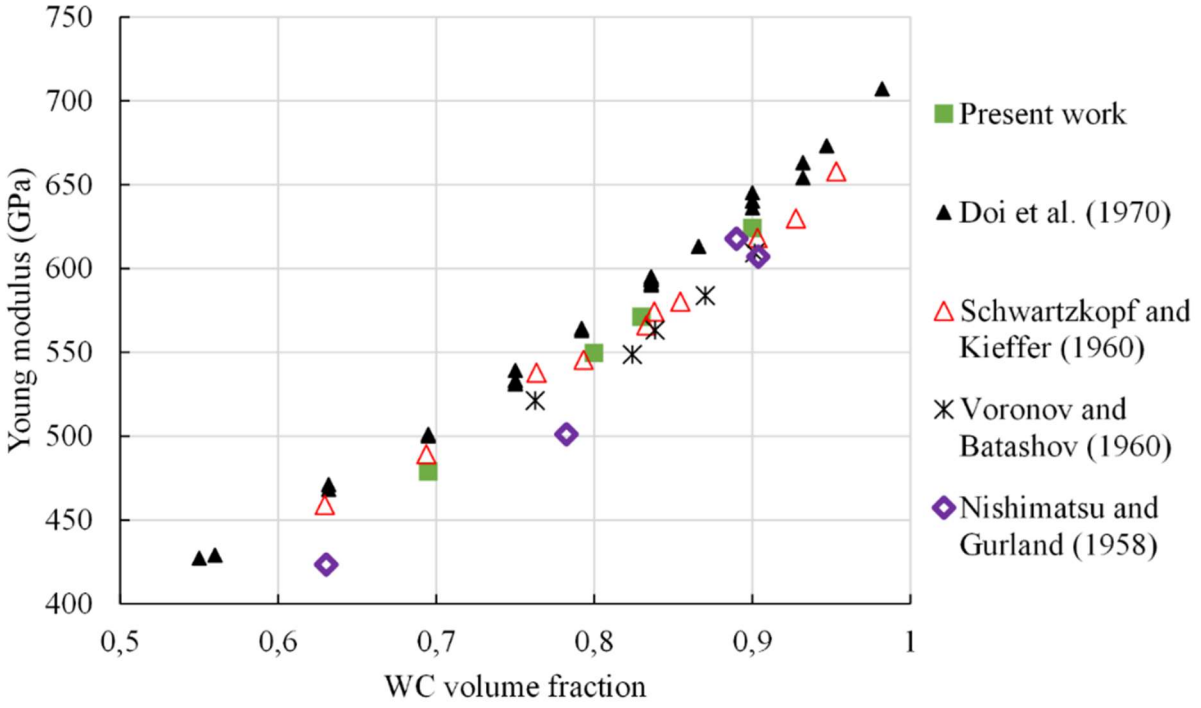

647

648 Figure 12. Comparison between the simulated Young's modulus for WC-Co with different WC
649 volume fractions and experimental results [48–51].

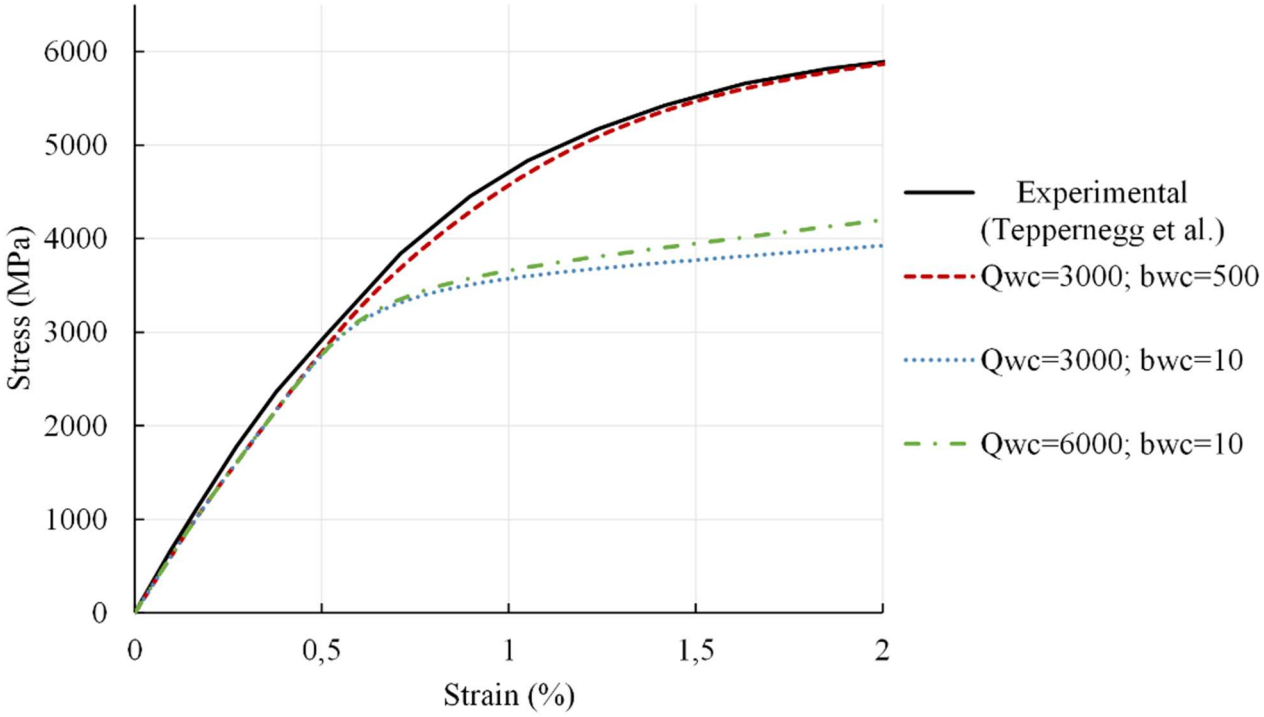

650

651 Figure 13. Influence of the hardening parameters Q_{WC} and b_{WC} on the computed stress-strain curves
652 for a composite WC-6wt.%Co in uniaxial compressive test.

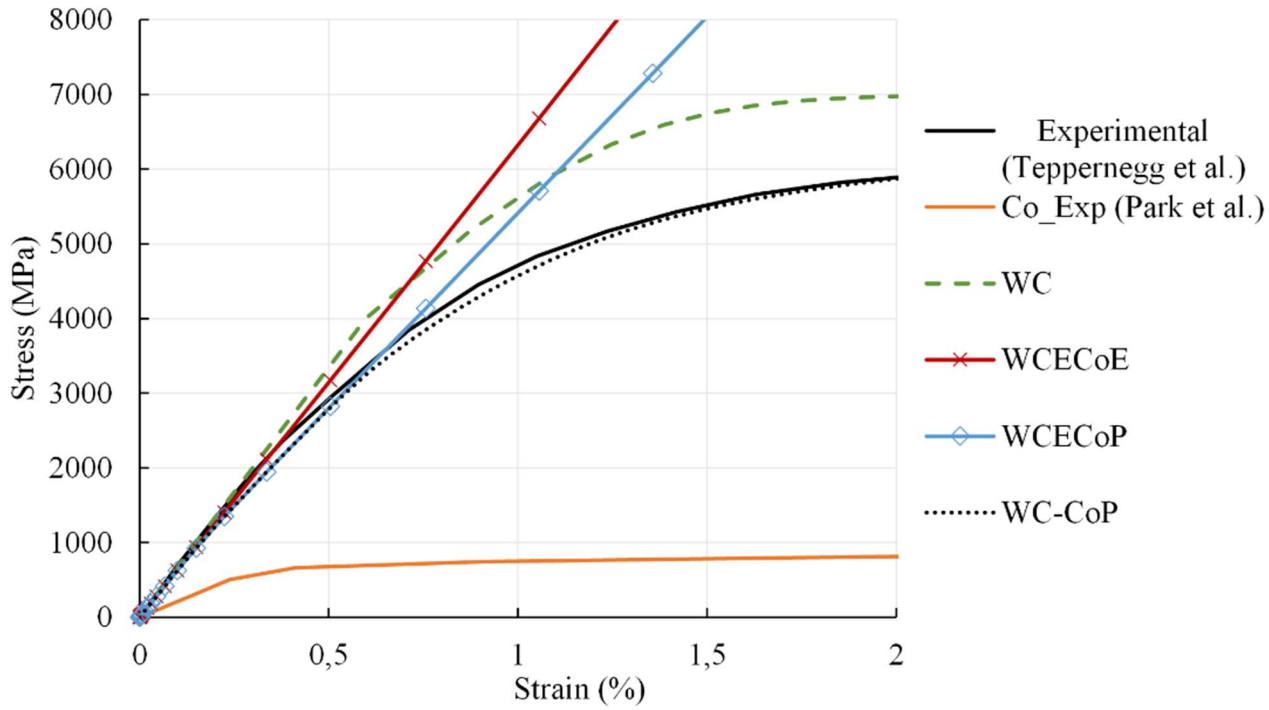

Figure 14. Comparison between the stress-strain curves for different combinations of phase behaviour in uniaxial compression with experimental data taken from references [30] and [38]. The indices E and P mean that the phases have elastic and elasto-plastic behaviours, respectively. For the WC phase, the selected hardening parameters are Q_{WC}=3000MPa and bwc=500.

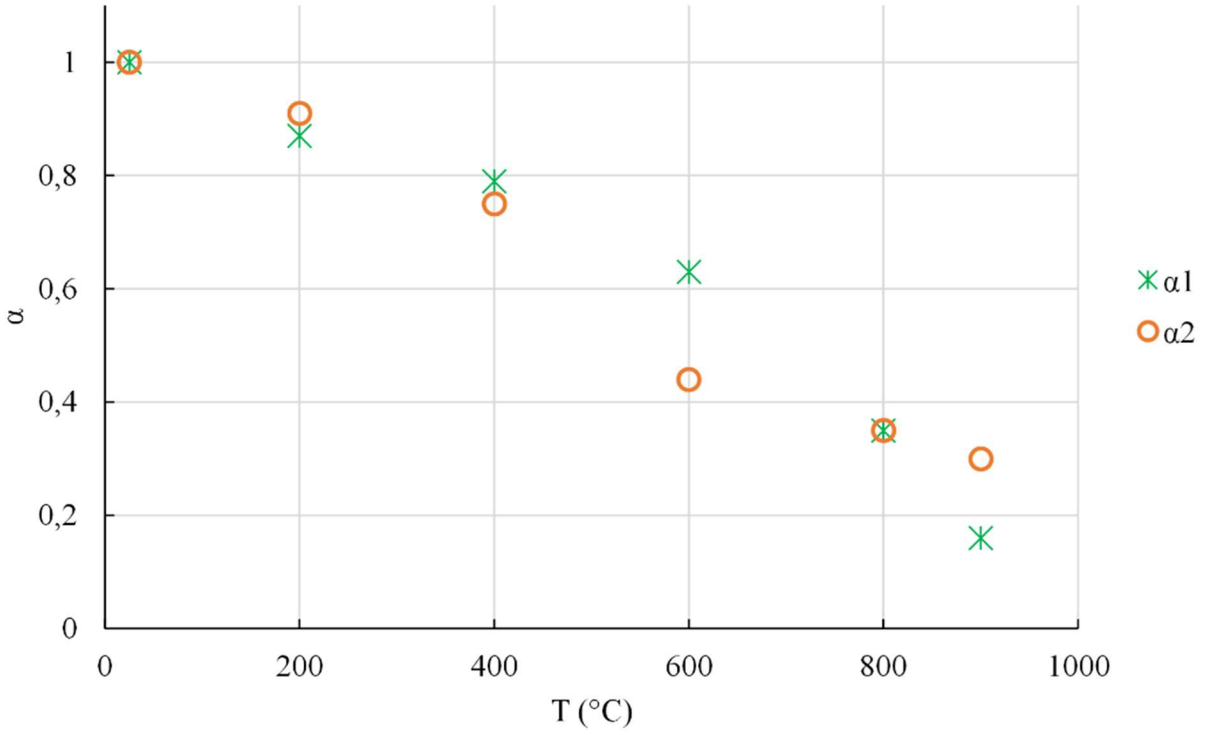

Figure 15. Evolution of α_1 and α_2 parameters as a function of temperature.

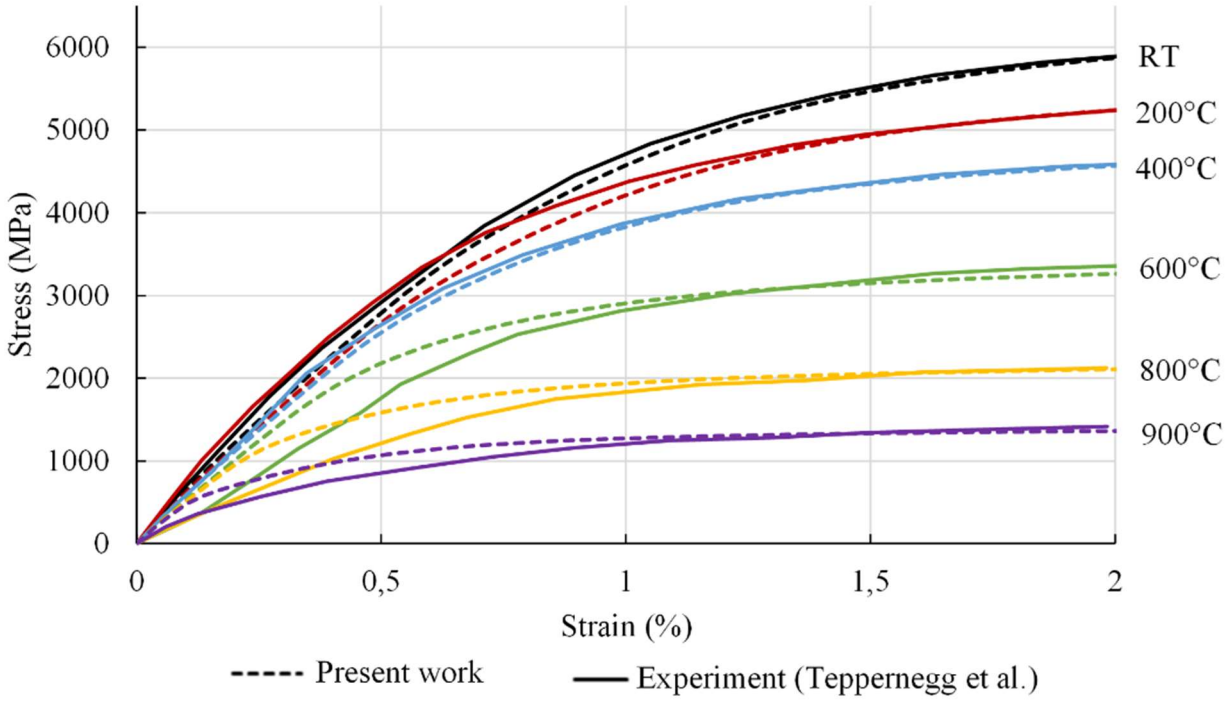

Figure 16. Comparison between experimental results obtained from [30] and computed stress-strain curves at different temperatures for a composite WC-6wt.%Co under uniaxial compression (200°C-900°C).

Table 1 Summary of the model parameters.

Cobalt (C_o)		
Young's modulus	E_{C_o}	See Figure 1
Poisson's ratio	ν_{C_o}	0.31 [21]
Coefficient of the thermal expansion	$\alpha_{T_{C_o}}$	See Figure 1
Initial yield stress and hardening		See Figure 3
Tungsten carbide (WC)		
Young's modulus	E_{WC}	See Figure 2
Poisson's ratio	ν_{WC}	0.194 [21]
Coefficient of the thermal expansion	$\alpha_{T_{WC}}$	See Figure 2
Von Mises and Drucker Prager models		
Initial yield stress in uniaxial compression	R_{WC}	4000 MPa [24]
Friction angle	ϕ_{WC}	45°
Dilatation angle	ψ_{WC}	45°
Hardening constants	Q_{WC}	3000 MPa
	b_{WC}	500

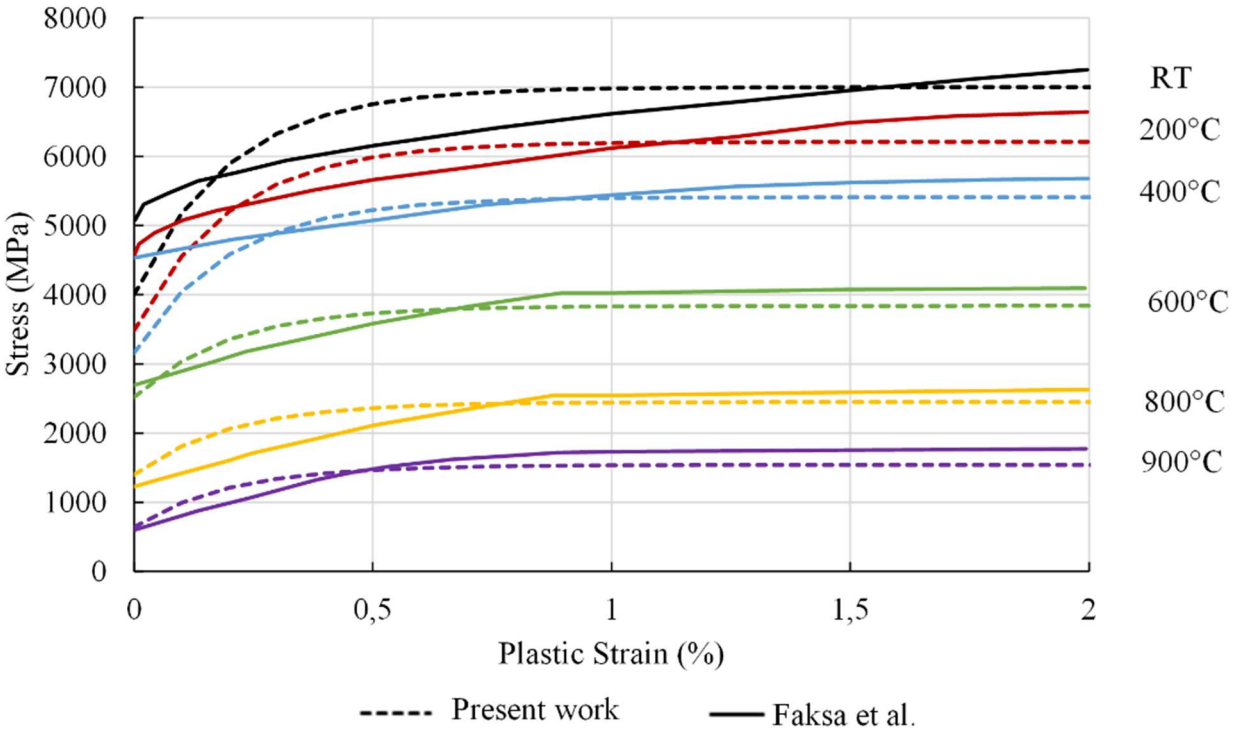

668

669 Figure 17. Comparison between stress-plastic strain curves computed in the present work and by
670 Faksa et al. [26] for the WC phase for different temperatures (200°C-900°C).

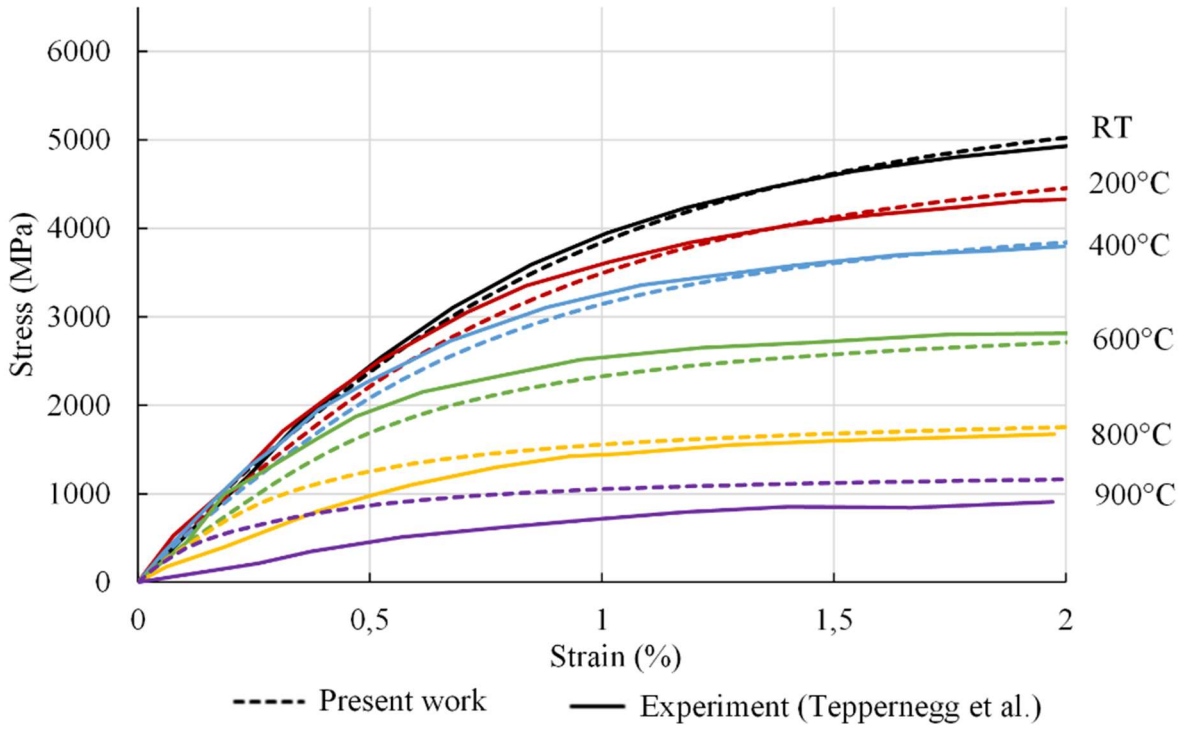

671

672 Figure 18. Comparison between the stress-strain curves computed in the present work and those
673 measured by Teppernegg et al. [30] for a composite WC-10.5wt.%Co under uniaxial compression for
674 different temperatures (200°C-900°C).

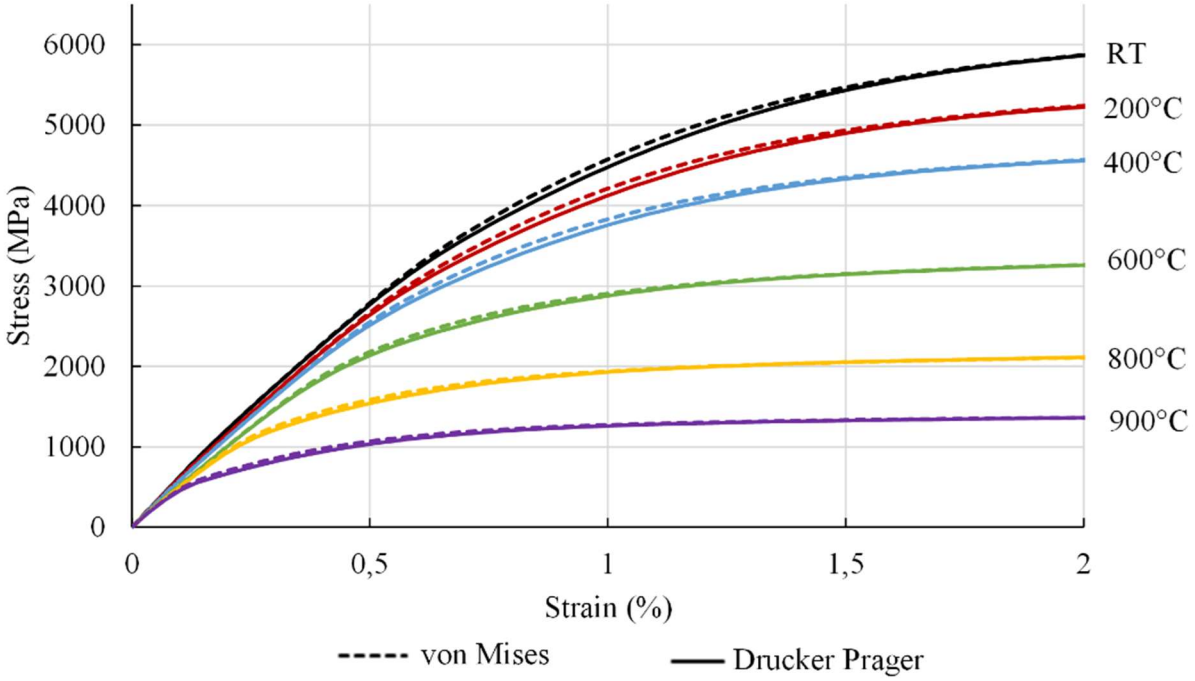

675

676 Figure 19. Comparison between the stress-strain curves computed with von Mises and Drucker Prager
677 models applied to the tungsten carbide phase for a composite WC-6wt.%Co under uniaxial
678 compression for different temperatures (200°C-900°C).

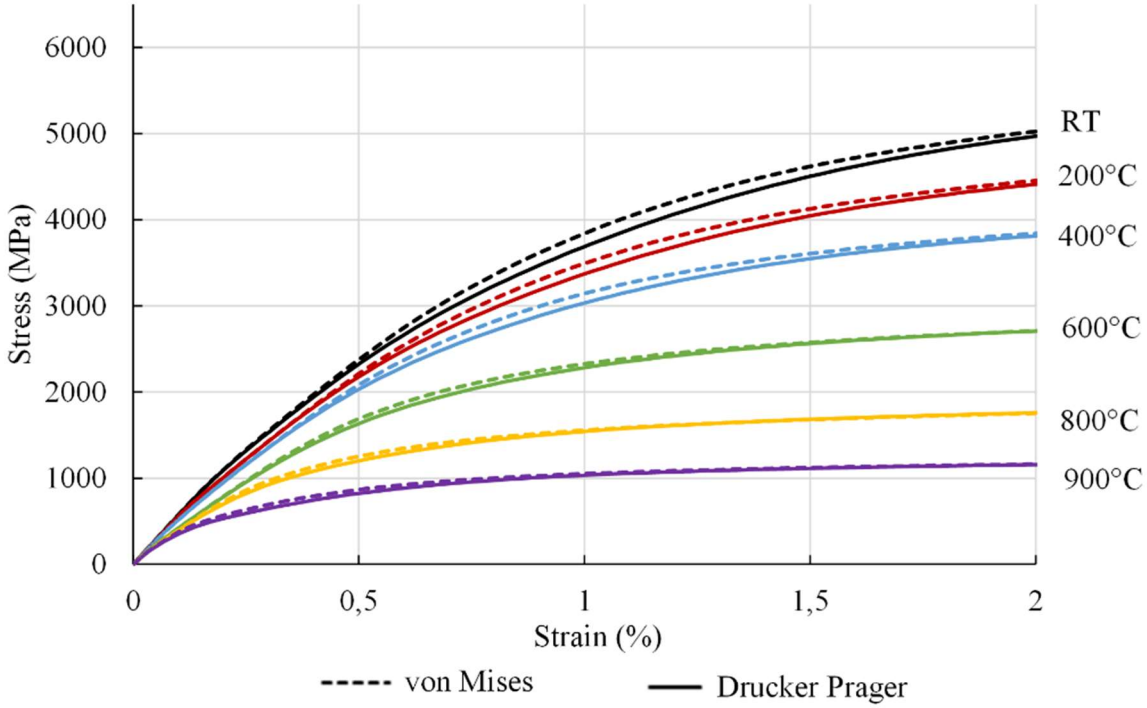

679

680 Figure 20. Comparison between the stress-strain curves computed with Mises and Drucker Prager
681 models applied to the tungsten carbide phase for a composite WC-10.5wt.%Co in uniaxial
682 compression for different temperatures.

683

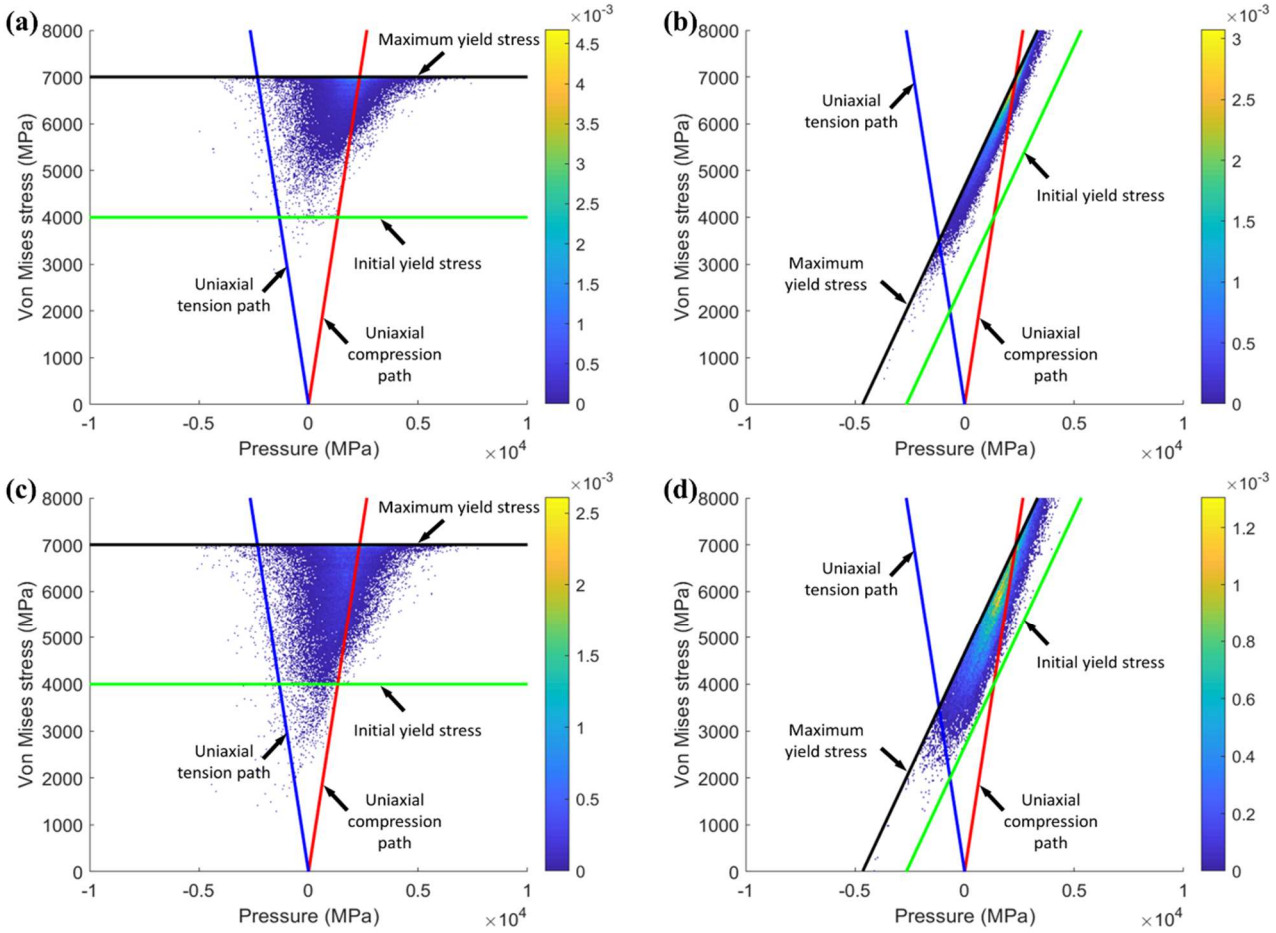

684

685 Figure 21. p-J2 Diagram obtained from the stress tensor calculated at each integration point in the
686 carbide phase. p is the pressure and J2 the von Mises stress. Each "point" in the figure corresponds to a
687 rectangle with dimensions of 50x25MPa containing a stress state group. The color of the scale
688 indicates the probability of finding this stress state group in the carbide phase. These data were
689 computed with (a): the von Mises criterion and (b): the Drucker Prager criterion for a WC-6wt.%Co
690 composite, (c): The von Mises criterion and (d) the Drucker Prager criterion for a WC-10.5wt.%Co
691 composite and for a total strain of 2% at room temperature.

References

[1] Z. Z. Fang, M. C. Koopman, and H. Wang, "Cemented Tungsten Carbide Hardmetal-An Introduction," in *Comprehensive Hard Materials*, vol. 1, Elsevier, 2014, pp. 123–137.

[2] G. Schneider, *Principles of tungsten carbide engineering: Expanded and up-dated to include ceramics*. Society of Carbide and Tool Engineers, 1989.

[3] H. E. Exner, "Physical and chemical nature of cemented carbides," *Int. Met. Rev.*, vol. 24, no. 1, pp. 149–173, 1979, doi: 10.1179/imtr.1979.24.1.149.

[4] P. E. McHugh and P. J. Connolly, "Micromechanical modelling of ductile crack growth in the binder phase of WC-Co," *Comput. Mater. Sci.*, vol. 27, no. 4, pp. 423–436, 2003, doi: 10.1016/S0927-0256(03)00045-4.

[5] T. Kresse, D. Meinhard, T. Bernthaler, and G. Schneider, "Hardness of WC-Co hard metals: Preparation, quantitative microstructure analysis, structure-property relationship and modelling," *Int. J. Refract. Met. Hard Mater.*, vol. 75, no. May, pp. 287–293, 2018, doi: 10.1016/j.ijrmhm.2018.05.003.

[6] J. García, V. Collado Ciprés, A. Blomqvist, and B. Kaplan, "Cemented carbide microstructures: a review," *Int. J. Refract. Met. Hard Mater.*, vol. 80, no. August 2018, pp. 40–68, 2019, doi: 10.1016/j.ijrmhm.2018.12.004.

[7] K. S. Ravichandran, "Fracture toughness of two phase WC-Co cermets," *Acta Metall. Mater.*, vol. 42, no. 1, pp. 143–150, 1994, doi: 10.1016/0956-7151(94)90057-4.

[8] P. Connolly and P. E. McHugh, "Fracture modelling of WC-Co hardmetals using crystal plasticity theory and the Gurson model," *Fatigue Fract. Eng. Mater. Struct.*, vol. 22, no. 1, pp. 77–86, 1999, doi: 10.1046/j.1460-2695.1999.00153.x.

[9] S. Herd, R. J. K. Wood, J. A. Wharton, and C. F. Higgs, "Explicit fracture modelling of cemented tungsten carbide (WC-Co) at the mesoscale," *Mater. Sci. Eng. A*, vol. 712, no. May 2017, pp. 521–530, 2018, doi: 10.1016/j.msea.2017.11.109.

[10] J. T. Smith and J. D. Wood, "Elevated temperature compressive creep behavior of tungsten carbide-cobalt alloys," *Acta Metall.*, vol. 16, no. 10, pp. 1219–1226, 1968.

[11] F. Ueda, H. Doi, F. Fujiwara, and H. Masatomi, "Bend deformation and fracture of WC-Co alloys at elevated temperatures.," *Trans Jpn Inst Met*, vol. 18, no. 3, pp. 247–256, 1977, doi: 10.2320/matertrans1960.18.247.

[12] M. M. Karimi, U. U. Gomes, M. P. Oliveira, R. D. S. Guimarães, M. M. B. Mello, and M. Filgueira, “Fracture toughness evaluation of WC–10 wt% Co hardmetal sintered under high pressure and high temperature,” *High Press. Res.*, vol. 37, no. 1, pp. 59–69, 2017, doi: 10.1080/08957959.2016.1261403.

[13] M. A. Davies, A. L. Cooke, and E. R. Larsen, “High bandwidth thermal microscopy of machining AISI 1045 steel,” *CIRP Ann. - Manuf. Technol.*, vol. 54, no. 1, pp. 63–66, 2005, doi: 10.1016/S0007-8506(07)60050-X.

[14] S. V. Emani, A. F. C. Ramos Dos Santos, L. L. Shaw, and Z. Chen, “Investigation of microstructure and mechanical properties at low and high temperatures of WC-6 wt% Co,” *Int. J. Refract. Met. Hard Mater.*, vol. 58, pp. 172–181, 2016, doi: 10.1016/j.ijrmhm.2016.04.009.

[15] D. Mari, “Déformation à haute température des composites WC-Co,” no. January 1991, 2014, doi: 10.5075/epfl-thesis-938.

[16] K. H. G. Ashbee, “Intersecting stacking faults in face-centered cubic lattices,” *Acta Metall.*, vol. 15, no. 7, pp. 1129–1131, 1967.

[17] U. A. Özden, K. Jiang, A. Bezold, and C. Broeckmann, “Evaluation of Fatigue Crack Growth Performance in different Hardmetal Grades based on Finite Element Simulation,” *Procedia Struct. Integr.*, vol. 2, pp. 648–655, 2016, doi: 10.1016/j.prostr.2016.06.084.

[18] H. F. Fischmeister, S. Schmauder, and L. S. Sigl, “Finite element modelling of crack propagation in WC-Co hard metals,” *Mater. Sci. Eng. A*, vol. 105, pp. 305–311, 1988.

[19] B. O. Jaensson and B. O. Sundström, “Determination of Young’s modulus and poisson’s ratio for WCCo alloys by the finite element method,” *Mater. Sci. Eng.*, vol. 9, no. C, pp. 217–222, 1972, doi: 10.1016/0025-5416(72)90036-5.

[20] B. O. Sundstrom, “Elastic-Plastic Behaviour of WC-Co Analysed by Continuum Mechanics,” vol. 12, 1973.

[21] M. H. Poech, H. F. Fischmeister, D. Kaute, and R. Spiegler, “FE-modelling of the deformation behaviour of WC-Co alloys,” *Comput. Mater. Sci.*, vol. 1, no. 3, pp. 213–224, 1993, doi: 10.1016/0927-0256(93)90013-D.

[22] T. Sadowski and T. Nowicki, “Numerical investigation of local mechanical properties of WC/Co composite,” *Comput. Mater. Sci.*, vol. 43, no. 1, pp. 235–241, 2008, doi: 10.1016/j.commatsci.2007.07.030.

[23] G. Chen, U. A. Ozden, A. Bezold, and C. Broeckmann, “A statistics based numerical

753 investigation on the prediction of elasto-plastic behavior of WC-Co hard metal," *Comput.*
754 *Mater. Sci.*, vol. 80, pp. 96–103, 2013, doi: 10.1016/j.commatsci.2013.04.004.

755 [24] D. Tkalich, G. Cailletaud, V. A. Yastrebov, and A. Kane, "A micromechanical constitutive
756 modeling of WC hardmetals using finite-element and uniform field models," *Mech. Mater.*,
757 vol. 105, pp. 166–187, 2017, doi: 10.1016/j.mechmat.2016.11.007.

758 [25] D. Tkalich, V. A. Yastrebov, G. Cailletaud, and A. Kane, "Multiscale modeling of cemented
759 tungsten carbide in hard rock drilling," *Int. J. Solids Struct.*, vol. 128, pp. 282–295, 2017, doi:
760 10.1016/j.ijsolstr.2017.08.034.

761 [26] L. Faksa *et al.*, "Shot peening-induced plastic deformation of individual phases within a coated
762 WC-Co hard metal composite material including stress-strain curves for WC as a function of
763 temperature," *Surf. Coatings Technol.*, vol. 380, no. September, p. 125026, 2019, doi:
764 10.1016/j.surfcoat.2019.125026.

765 [27] J. Weidow and H. O. Andrén, "Binder phase grain size in WC-Co-based cemented carbides,"
766 *Scr. Mater.*, vol. 63, no. 12, pp. 1165–1168, 2010, doi: 10.1016/j.scriptamat.2010.08.025.

767 [28] W. Betteridge, "The properties of metallic cobalt," *Prog. Mater. Sci.*, vol. 24, no. C, pp. 51–
768 142, 1980, doi: 10.1016/0079-6425(79)90004-5.

769 [29] M. E. Fine and W. C. Ellis, "Thermal expansion properties of iron-cobalt alloys," *Trans. Am.*
770 *Inst. Min. Met. Eng.*, vol. 175, p. 742, 1948.

771 [30] T. Teppernegg *et al.*, "High temperature mechanical properties of WC-Co hard metals," *Int. J.*
772 *Refract. Met. Hard Mater.*, vol. 56, pp. 139–144, 2016, doi: 10.1016/j.ijrmhm.2016.01.002.

773 [31] J. fei Zhu, L. Zhang, H. dong Zhang, Z. qiang Zhong, L. Zhou, and Y. Chen, "Real
774 microstructure-based simulation of thermal residual stresses in cemented carbides and the
775 related strengthening and toughening consideration," *Int. J. Refract. Met. Hard Mater.*, vol. 71,
776 no. November 2017, pp. 239–245, 2018, doi: 10.1016/j.ijrmhm.2017.11.014.

777 [32] T. Sadowski, S. J. Hardy, and E. W. Postek, "Prediction of the mechanical response of
778 polycrystalline ceramics containing metallic intergranular layers under uniaxial tension,"
779 *Comput. Mater. Sci.*, vol. 34, no. 1, pp. 46–63, 2005, doi: 10.1016/j.commatsci.2004.10.005.

780 [33] R. R. Reeber and K. Wang, "Thermophysical Properties of Tungsten Carbide," vol. 35, 1999.

781 [34] T. Takahashi and E. J. Freise, "Determination of the slip systems in single crystals of tungsten
782 monocarbide," *Philos. Mag.*, vol. 12, no. 115, pp. 1–8, 1965, doi:
783 10.1080/14786436508224941.

[35] M. K. Hibbs and R. Sinclair, “Room-temperature deformation mechanisms and the defect structure of tungsten carbide,” *Acta Metall.*, vol. 29, no. 9, pp. 1645–1654, 1981.

[36] V. K. Sarin and T. Johannesson, “On the deformation of WC--Co cemented carbides,” *Met. Sci.*, vol. 9, no. 1, pp. 472–476, 1975.

[37] V. Abaqus, “6.14 Documentation,” *Dassault Syst. Simulia Corp.*, vol. 651, pp. 2–6, 2014.

[38] S. Park, S. G. Kapoor, and R. E. DeVor, “Microstructure-level model for the prediction of tool failure in WC-Co cutting tool materials,” *J. Manuf. Sci. Eng.*, vol. 128, no. 3, pp. 739–748, 2006.

[39] D. C. Drucker and W. Prager, “Soil mechanics and plastic analysis or limit design,” *Q. Appl. Math.*, vol. 10, no. 2, pp. 157–165, 1952.

[40] H. Doi, *Elastic and Plastic Properties of WC-Co Composite Alloys*. Freund Publishing House, 1974.

[41] M. Christensen and G. Wahnström, “Effects of cobalt intergranular segregation on interface energetics in WC-Co,” *Acta Mater.*, vol. 52, no. 8, pp. 2199–2207, 2004, doi: 10.1016/j.actamat.2004.01.013.

[42] T. Csanádi, M. Vojtko, and J. Dusza, “Deformation and fracture of WC grains and grain boundaries in a WC-Co hardmetal during microcantilever bending tests,” *Int. J. Refract. Met. Hard Mater.*, vol. 87, no. July 2019, p. 105163, 2020, doi: 10.1016/j.ijrmhm.2019.105163.

[43] W. Dawihl and J. Hinnüber, “Über den Aufbau der Hartmetallegierungen,” *Kolloid-Zeitschrift*, vol. 104, no. 2, pp. 233–236, Sep. 1943, doi: 10.1007/BF01519451.

[44] E. Jiménez-Piqué *et al.*, “Focused ion beam tomography of WC-Co cemented carbides,” *Int. J. Refract. Met. Hard Mater.*, vol. 67, no. April, pp. 9–17, 2017, doi: 10.1016/j.ijrmhm.2017.04.007.

[45] G. List, “Etude des mécanismes d’endommagement des outils carbure WC-Co par la caractérisation de l’interface outil copeau: application à l’usinage à sec de l’alliage d’aluminium aéronautique AA2024 T351,” Paris, ENSAM, 2004.

[46] W. Kayser, A. Bezold, and C. Broeckmann, “Simulation of residual stresses in cemented carbides,” *Int. J. Refract. Met. Hard Mater.*, vol. 63, pp. 55–62, 2017, doi: 10.1016/j.ijrmhm.2016.04.001.

[47] E. Postek and T. Sadowski, “Dynamic pulse sensitivity of WC/Co composite,” *Compos.*

Struct., vol. 203, no. July 2017, pp. 498–512, 2018, doi: 10.1016/j.compstruct.2017.10.092.

[48] P. Schwarzkopf and R. Kieffer, *Cemented carbides*. Macmillan, 1960.

[49] F. Voronov and D. Balashov, "The adiabatic moduli of elasticity in sintered tungsten carbide cutting alloys," *Phys. Met. Met.*, vol. 9, no. 4, pp. 127–130, 1960.

[50] C. Nishimatsu and J. Gurland, "Experimental survey of the deformation of a hard-ductile two-phase alloy system (WC-CO)," 1958.

[51] H. Doi, Y. Fujiwara, K. Miyake, and Y. Oosawa, "A systematic investigation of elastic moduli of Wc-Co alloys," *Metall. Mater. Trans.*, vol. 1, no. 5, pp. 1417–1425, 1970, doi: 10.1007/BF02900264.

[52] N. Hansen, "Hall-petch relation and boundary strengthening," *Scr. Mater.*, vol. 51, no. 8 SPEC. ISS., pp. 801–806, 2004, doi: 10.1016/j.scriptamat.2004.06.002.

[53] F. De Luca *et al.*, "Nanomechanical Behaviour of Individual Phases in WC-Co Cemented Carbides, from Ambient to High Temperature.," *Materialia*, vol. 12, no. May, 2020, doi: 10.1016/j.mtla.2020.100713.

[54] M. A. Yousfi, J. Weidow, A. Nordgren, L. K. L. Falk, and H. O. Andrén, "Deformation mechanisms in a WC-Co based cemented carbide during creep," *Int. J. Refract. Met. Hard Mater.*, vol. 49, no. 1, pp. 81–87, 2015, doi: 10.1016/j.ijrmhm.2014.07.016.

[55] T. Csanádi, M. Bľanda, A. Duszová, N. Q. Chinh, P. Szommer, and J. Dusza, "Deformation characteristics of WC micropillars," *J. Eur. Ceram. Soc.*, vol. 34, no. 15, pp. 4099–4103, 2014, doi: 10.1016/j.jeurceramsoc.2014.05.045.

[56] T. Sakuma and H. Hondo, "Plastic flow in WC-13wt.%Co at high temperatures," *Mater. Sci. Eng. A*, vol. 156, no. 2, pp. 125–130, 1992, doi: 10.1016/0921-5093(92)90144-P.

[57] W. Koster, "The Temperature Dependence of the Elastic Modulus of Pure Metals," *Ztsch. für Met.*, vol. 39, p. 1, 1948.